2

Quinazoline and Quinoline-Based Small Molecules as Utrophin Upregulators for Duchenne Muscular Dystrophy

2.1 Abstract

Duchenne muscular dystrophy (DMD) is a progressive and fatal muscle-wasting disorder caused by mutations in the DMD gene, leading to an absence of functional dystrophin protein. Since dystrophin is crucial for maintaining muscle integrity, its deficiency results in severe muscle degeneration. A mutation-independent therapeutic strategy involves the upregulation of utrophin, a structural and functional paralog of dystrophin, which can compensate for dystrophin loss. This approach offers a universal treatment strategy, regardless of the specific underlying mutations in the DMD gene.

In this study, we report the design and synthesis of novel Quinazoline- and Quinoline-based small molecules as potent utrophin modulators. A library of seventy compounds was synthesized and further screened using a high-throughput In-Cell ELISA assay in C2C12 cells to identify lead molecules capable of elevating utrophin expression. Among these, SG-02 emerged as a lead compound with remarkable activity, demonstrating a 2.7-fold upregulation of utrophin at a nanomolar concentration (800 nM) in a dose-dependent manner. The therapeutic potential of SG-02 was further evaluated in clinically relevant DMD patient-derived cells, where it showed a significant 2.3-fold increase in utrophin expression. Mechanistic studies identified SG-02 as a potent antagonist of the aryl hydrocarbon receptor (AhR). SG-02 exhibited high binding affinity to AhR, with a dissociation constant (K_d) of 41.68 nM, indicating strong target engagement. Additionally, SG-02 was found to enhance myogenesis, as evidenced by increased expression of myosin heavy chain (MyHC), a myogenic marker for muscle differentiation. Preliminary evaluation of ADME properties, supports candidature of SG-02 as an oral bioavailable therapeutics.

This study introduce SG-02 as a promising small-molecule therapeutics for DMD that targets utrophin upregulation via AhR antagonism. SG-02 holds the potential to benefit the entire DMD population.

2.2 Introduction

Duchenne muscular dystrophy (DMD) is a severe and progressive genetic disorder characterized by muscle degeneration and weakness, affecting approximately 1 in 3,500 males detailed in introduction chapter under section 1.1 and 1.2.[1-5]

This chapter focuses on the development of cost-effective, orally bioavailable therapeutics aimed at treating the global population of DMD patients. To this direction, we first review the currently available DMD treatments and their limitations. The discovery of the DMD gene[6] has spurred various therapeutic strategies,[7] including approved treatments like ataluren (for premature stop-codon read-through) and exon-skipping drugs, such as Eteplirsen (targeting exon 51) and Golodirsen (targeting exon 53), address specific genetic mutations,[8] benefiting only a subset of patients. Gene therapy approaches, including viral vector-based delivery and CRISPR/Cas9 gene editing, are being actively explored but face challenges related to delivery efficiency, immune responses, and mutation coverage.[9] In most cases, DMD management still relies on symptomatic treatments, such as corticosteroids, to reduce inflammation and fibrosis. Although these treatments marginally improve life expectancy, no current therapy can alter disease progression or address the universal DMD population.[8-11] Thus, there remains an urgent need for therapeutic approaches that can benefit all DMD patients.

A promising alternative strategy is the upregulation of utrophin, a structural and functional homolog of dystrophin, as a mutation-independent approach. Utrophin is naturally expressed during foetal development and can compensate for dystrophin deficiency when re-expressed in sufficient levels.[12] Research suggests that a 2- to 3-fold increase in utrophin can partially or completely mitigate the dystrophic phenotype and restore muscle function.[13] The advantage of utrophin-based therapy lies in its universal applicability to all patients regardless of genetic mutation[10] and its lack of requirement for immunosuppression.[14] Preclinical studies have demonstrated that expressing truncated or full-length utrophin in the mdx mouse model alleviates DMD pathology.[13-15] Moreover, clinical observations in DMD patients show increased utrophin expression with age, potentially slows disease progression and acts as a compensatory mechanism.[16] These findings establish utrophin upregulation as a viable therapeutic avenue for DMD.

Initial clinical efforts targeting utrophin included the development of Ezutromid, an orally bioavailable drug by Summit Therapeutics, designed to activate the utrophin-A promoter.[17], Ezutromid exhibits promising results in early trials but failed in later stages of clinical studies in phase-II due to poor metabolism. Subsequently, a second-generation utrophin modulator, SMT022357, was developed, offering a more stable metabolic profile and improved pharmacokinetics.[18] Mechanistic studies revealed that Ezutromid acts as an aryl hydrocarbon receptor (AhR) antagonist, and parallel study with other AhR antagonists have also revealed the potential to upregulate utrophin. This discovery highlighted AhR modulation as a potential pathway for DMD therapeutics.[19]

Building on these findings, we designed and synthesized a novel series of quinazoline- and quinoline-based small molecules to enhance utrophin expression via AhR antagonism, distinct from the Ezutromid benazoxazole scaffold. These molecules were designed by exploring known AhR antagonist ligands and other compounds capable of modulating utrophin expression. Our series demonstrated potent activity, achieving significant utrophin

upregulation at nanomolar concentrations. These molecules represent a potential breakthrough in DMD treatment by offering a novel utrophin modulator with highest fold change at lower concentration.[20-21] Library of 70 was synthesized and further screened through a high-throughput In-Cell ELISA technique in C2C12 mouse myoblast cell line. This assay allowed precise, quantitative measurement of intracellular utrophin without cell lysis. The identified lead candidate 'SG-02' showed a remarkable 2.7-fold increase in utrophin protein expression and a 2.11-fold increase in mRNA levels at 800 nM, validated through qRT-PCR and Western blot analysis. To further check the potency of the lead candidate SG-02 in clinically relevant human DMD patient-derived cell line KM1328, the findings from these experiments supports SG-02 candidature for DMD therapy as it demonstrated a 2.3-fold increase in utrophin protein levels at the same optimum concentration of 800 nM.

Mechanistic investigations confirmed that SG-02 functions via AhR antagonism, as evidenced by its high binding affinity (K_d = 41.68 nM) and co-localization studies with the AhR agonist ligand ITE (2-(1′H-indole-3′-carbonyl)-thiazole-4-carboxylic acid methyl ester).[19] Additionally, SG-02 enhances myogenesis, the process by which myoblasts fuse to form mature myotubes, a critical step in muscle development and repair. Immunocytochemical analysis of myosin heavy chain (MyHC) expression in the C2C12 cell line demonstrated a nearly two fold increase in the fusion index, indicating enhanced myotube formation. These findings highlight SG-02's potential to restore muscle function and facilitate repair processes, which are compromised in DMD patients.[22-24]

Preliminary evaluation of ADME (absorption, distribution, metabolism, and excretion) properties of lead candidate SG-02 indicated favourable pharmacokinetic properties, including oral bioavailability, supporting SG-02's candidacy as a drug for systemic oral administration. Overall, our findings suggest SG-02 as a potent and promising therapeutic candidate for DMD, capable of addressing the universal patient population through utrophin upregulation via AhR antagonism. This novel approach represents a significant step forward in the development of mutation-independent treatments for this devastating genetic disorder.

2.3 Results and Discussion

2.3.1 Design of Utrophin Modulators Based on Quinoline and Quinazoline scaffold

The basis of the design is depicted in (Figure 2.1 A&B). After the discovery of the mode of action for the first in-class utrophin modulator "Ezutromid" which targets AhR protein and acts as an antagonist, and the subsequent validation of other AhR antagonist's role in upregulating utrophin[19] inspired us to explore AhR antagonist ligands. Additionally, we have inspected some drugs both synthetically and naturally, which demonstrated utrophin upregulation capabilities.[20] On the basis of that, we have designed and synthesized our novel series of molecular library based on quinoline and quinazoline scaffolds. The analogy of choosing quinoline analogues were inspired from the drug nabumetone, which showed promising utrophin upregulation on drug repurposing studies.[20] However, due to the cardiac implications inherent in DMD pathology, the potential side effects of nabumetone, such as heart attack and stroke, restricted its direct application for treating DMD patients.[25] Here, we have replaced one carbon atom of the basic naphthalene moiety of nabumetone with a

nitrogen atom resulting in the development of quinoline scaffold. Additionally, an amine substitution was appended at the C-2 position, drawing inspiration from another drug phenazopyridine, known for its promising utrophin upregulation on drug repurposing studies.[20] To diversify the activity and efficacy, various active substituents were attached to the C-2 position of the quinoline scaffold with the help of an amine substitution. Similarly, the selection of quinazoline analogues was also guided from nabumetone. In this case, the basic core structure was modified by replacing two carbon atoms with nitrogen atoms, leading to the development of the quinazoline scaffold. This substitution was influenced from GNF-351, a recognized AhR antagonist capable of upregulating utrophin.[26] However, GNF-351 itself has limitations, particularly in terms of its bioavailability when administered orally, as it primarily localizes in the gastrointestinal tract.[27] In light of this, we aimed to design a new quinazoline-based scaffold that was inspired from both nabumetone and GNF-351. Based on a similar approach of amine substitution at C-2 position as discussed in the case of quinoline scaffold, different functional moieties were affixed here. The choice of ligands for the amine substitution at the C-2 position of both quinoline and quinazoline scaffold were based on exploring different AhR antagonist ligands and drug molecules having a potential for utrophin upregulation.[18-21] These rational design choices aimed to enhance the efficacy and utility of the quinazoline and quinoline analogues for utrophin upregulation. Furthermore, to enhance the aqueous solubility of the drug candidate and facilitate its potential as an orally bioavailable compound, an aqueous soluble motif was introduced at the C-6 and C-7-position of the quinoline and quinazoline scaffolds. Considering this, both methyl and ethyl substituents of sulfonyl moiety were taken.[17] Overall, this novel quinazoline and quinoline based small molecules were tailored made design guided from scientific insights, aiming to leverage potential therapeutic properties and come up with a novel utrophin modulator which could treat universal DMD population.

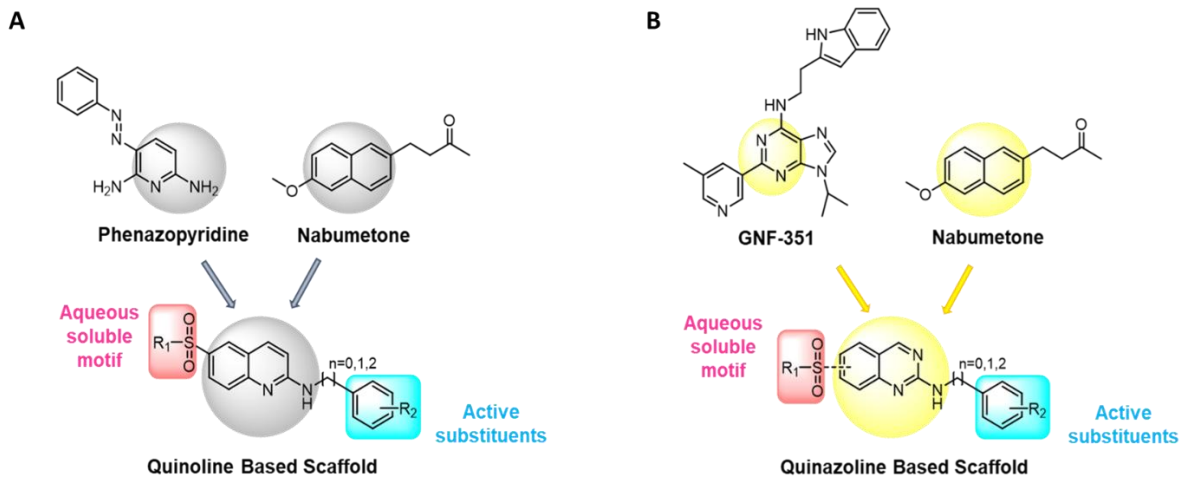


Figure 2.1: Design of tailor-made molecules having potential of utrophin modulation and molecular docking analysis. (A) Design of quinoline based scaffold from the structural features of phenazopyridine and nabumetone. (B) Design of quinazoline based scaffold from the structural features of GNF-351 and nabumetone.

2.3.2 In-silico Molecular Docking Analysis

The design concept of novel quinazoline and quinoline-based small molecules was subjected to preliminary in-silico validation prior to wet lab synthesis to ascertain their potential binding affinity to the target AhR protein. This validation involved conducting a molecular docking analysis between our designed molecules and the Aryl hydrocarbon receptor-mediated gene activation protein (PDB ID: 5NJ8) using Autodock Vina 1.1.2.36. Molecular docking analysis revealed that the designed series of library interacted with a specific pocket within the AhR protein structure, primarily through π−π stacking interaction. The lead molecule SG-02 identified when docked exhibits binding with the AhR protein through a network of interactions with binding affinity of -9.8 kcal/mol.

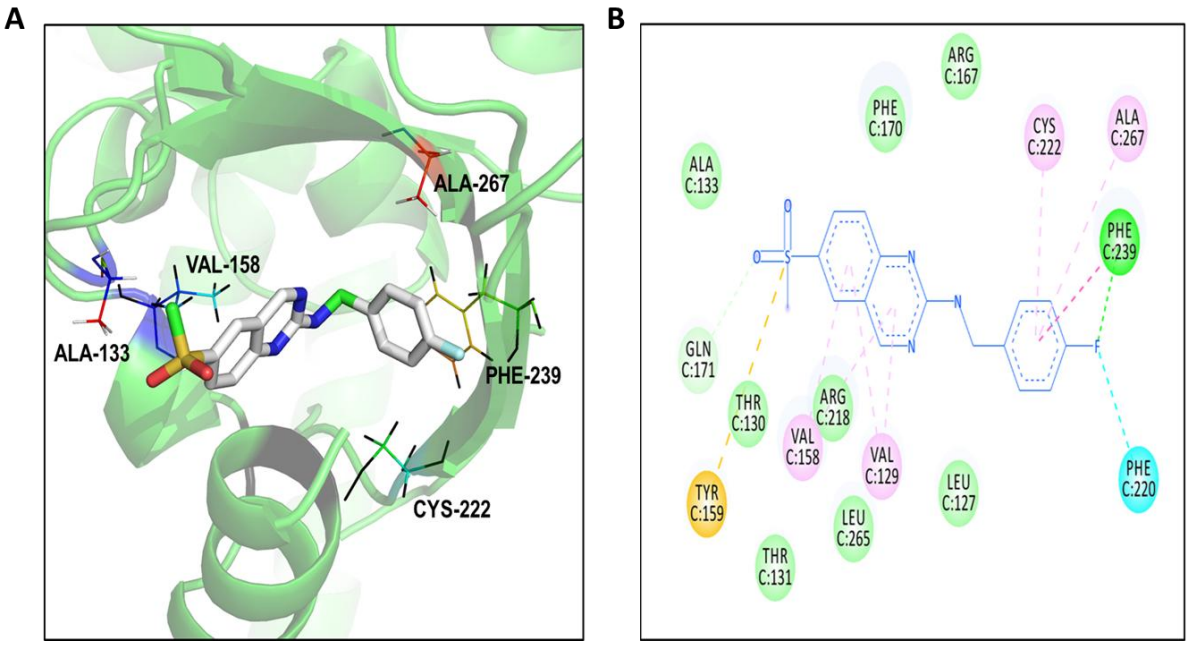


Figure 2.2: A) Binding model of SG-02 with AhR: ARNT complex protein (PDB ID: 5NJ8) showing possible binding interactions with key amino acids. (B) 2D binding interactions of compound SG-02 with the important amino acid residues. Pink circles reflects π−π stacking interaction, yellow circle represent pi-sulfur interaction and deep green circle indicates hydrogen bonding interaction of amino acid residues with ligand.

The ligand SG-02 established a binding interaction within a pocket of the AhR protein, engaging in π−π stacked interaction with Val-158, Val-129, Cys-222, and Ala-267 and participated in a pi-sulfur interaction with Tyr-159 due to the presence of a sulfonyl analogue in the core scaffold. Furthermore, SG-02 also formed conventional hydrogen bonding interactions with Phe-239, facilitated by the presence of a fluorine substitution. (Figure 2.2 A-B). Our analysis revealed that the designed molecules exhibited binding interactions with the AhR protein within the same binding pocket as Ezutromid, a first-in-class drug for utrophin upregulation targeting AhR protein.[17] (Figure 2.3 A-B).

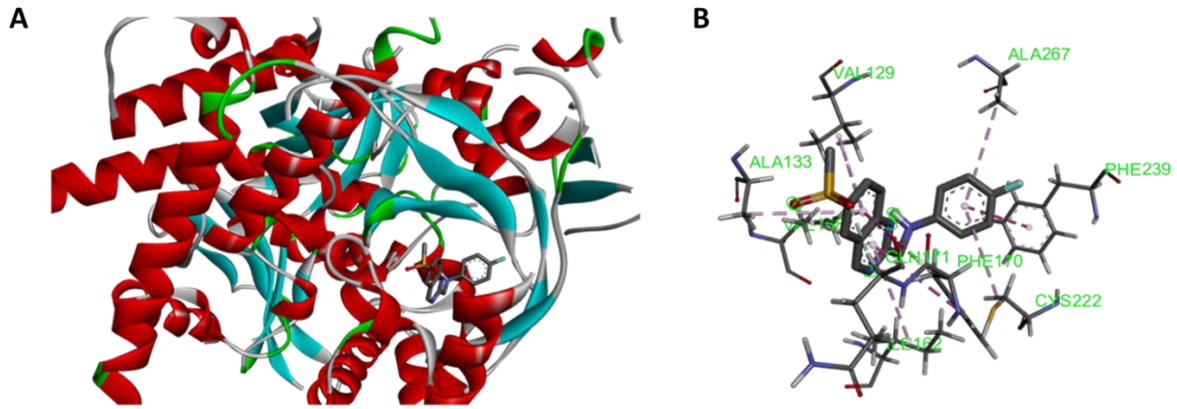
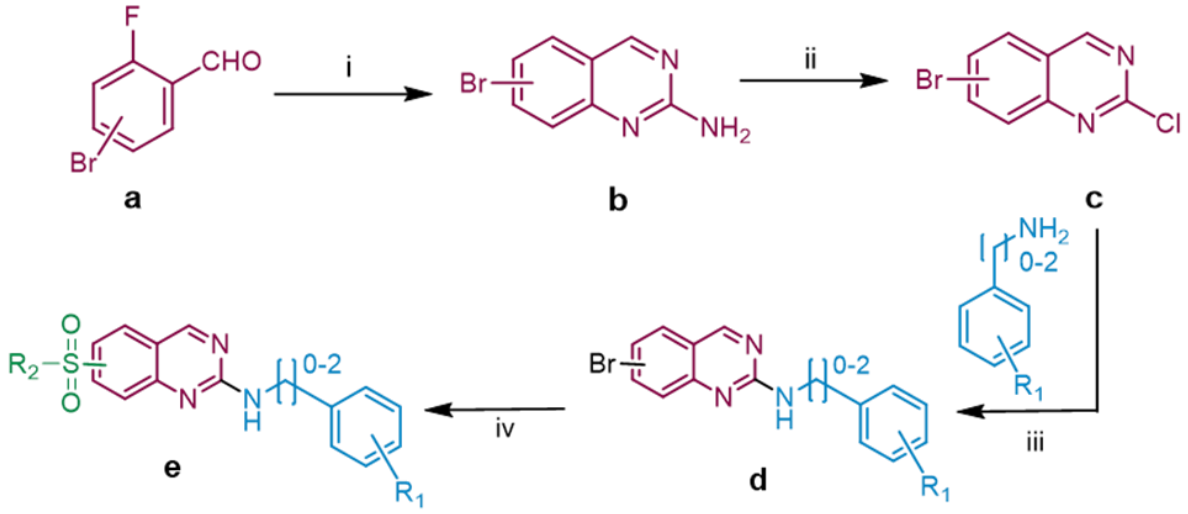


Figure 2.3: A) Binding site of lead molecule SG-02 with AhR:ARNT (PDBID: 5NJ8) protein complex. (B) Amino acid of protein interacting with SG-02.

2.3.3 Chemistry

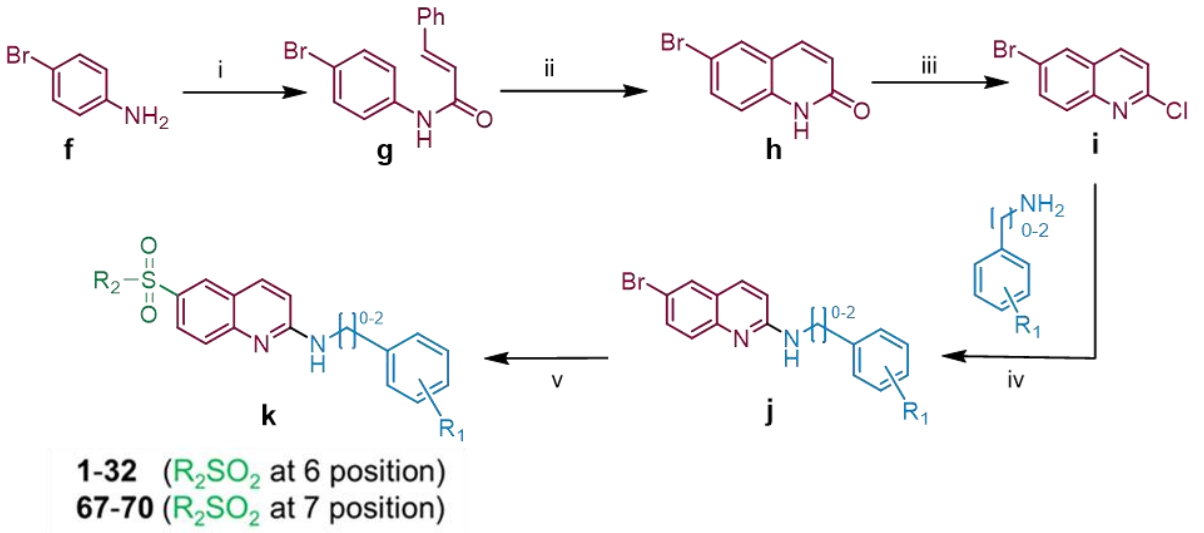
The designed quinazoline and quinoline scaffolds were synthesized using two distinct synthetic routes. For the quinazoline scaffold, a straightforward four-step synthetic strategy was employed, as depicted in (Scheme 1). The synthesis commenced with a cyclocondensation approach to generate the basic quinazoline motif with an amine substitution at the 2-position. Initially, 5-bromo-2-fluorobenzaldehyde was reacted with guanidine carbonate under reflux conditions, resulting in a good yield (72%) of 6/7-bromoquinazolin-2-amine. [28] Subsequently, the amine-substituted quinazoline motif was transformed into the corresponding chloro-substituted derivative (6-bromo-2-chloroquinazoline) using n-Bu_4NCl, TMSCl, and t-BuON=O reagents at 50 °C for 2-3 hr, providing a moderate yield (45%).[29] This step was carried out to enable the subsequent substitution of the chloro group with differently substituted library amines. The substitution reactions with diverse substituted amines were performed in ethanol at 150 °C for 12-24 hr in a sealed tube, yielding the desired products in good yield (88%).[30] Finally, to introduce the aqueous soluble sulfinate group, the bromo group at the C-6/C-7 position of the scaffold was replaced with (methyl/ethyl) sulfinate using copper iodide, L-proline, and K_2CO_3 at 130°C for 12 hr, yielding the final products in moderate to good yield (50-60%).[31]



1 n=0, R_1= F, R_2= Me	**13** n=0, R_1= 3,5-dimethoxy, R_2= Me	**25** n=1, R_1= OMe, R_2= Me
2 n=0, R_1= F, R_2= Et	**14** n=0, R_1= 3,5-dimethoxy, R_2= Me	**26** n=1, R_1= OMe, R_2= Et
3 n=0, R_1= CF_3, R_2= Me	**15** n=1, R_1= F, R_2= Me	**27** n=1, R_1= 3,5-dimethoxy, R_2= Me
4 n=0, R_1= CF_3, R_2= Et	**16** n=1, R_1= F, R_2= Et	**28** n=1, R_1= 3,5-dimethoxy, R_2= Et
5 n=0, R_1= OCH_2O, R_2= Me	**17** n=1, R_1= CF_3, R_2= Me	**29** n=1, R_1= Pyridine, R_2= Me
6 n=0, R_1= OCH_2O, R_2= Et	**18** n=1, R_1= CF_3, R_2= Et	**30** n=1, R_1= Pyridine, R_2= Et
7 n=0, R_1= OH, R_2= Me	**19** n=1, R_1= OCH_2O, R_2= Et	**31** n=2, R_1= Indole, R_2= Me
8 n=0, R_1= OH, R_2= Et	**20** n=1, R_1= OCH_2O, R_2= Et	**32** n=2, R_1= Indole, R_2= Et
9 n=0, R_1= $C(CH_3)3$, R_2= Me	**21** n=1, R_1= OH, R_2= Me	**67** n=1, R_1= F, R_2= Me
10 n=0, R_1= $C(CH_3)3$, R_2= Et	**22** n=1, R_1= OH, R_2= Et	**68** n=1, R_1= F, R_2= Et
11 n=0, R_1= OMe, R_2= Me	**23** n=1, R_1= $C(CH_3)3$, R_2= Me	**69** n=1, R_1= CF_3, R_2= Me
12 n=0, R_1= OMe, R_2= Et	**24** n=1, R_1= $C(CH_3)3$, R_2= Et	**70** n=1, R_1= CF_3, R_2= Et

Figure 2.4: Scheme 1: Routes employed towards synthesis of quinazoline analogues and library of molecules synthesized. Reagents and conditions: (i) Guanidine carbonate, DMA, Reflux, 5h (ii) n-Bu4NCl, TMSCL, t-BuON=O, DCM:DMF (8:2), 50 °C, 2-3h (iii) Ethanol, 150 °C (24-48h) (iv) RSO_2Na, CuI, L-Proline, K_2CO_3, DMSO, 130 °C, 12h.

For the synthesis of the quinoline scaffold, a distinct synthetic route was employed, as represented in Scheme 2. The synthesis began with a cyclocondensation approach to generate the quinoline scaffold, involving the formation of two key intermediates. The starting material used was 4-bromoaniline, which was reacted with cinnamoyl chloride to yield N-(4-bromophenyl) cinnamamide.[32] Subsequently, this intermediate was allowed to react with $AlCl_3$ under reflux condition in chlorobenzene solvent for 4-5 hr, resulting in the formation of 6-bromoquinolin-2(1H)-one. Next, the intermediate lactam was reacted with neat $POCl_3$ under reflux conditions for 1.5-2 hr to afford the 6-bromo-2-chloroquinoline in good yield (94%).[33] The subsequent steps involve the substitution of the chloro group with various amines and the attachment of the aqueous soluble sulfonyl group at the C-6 position, followed the same procedure as described earlier for the quinazoline scaffold in Scheme 1.



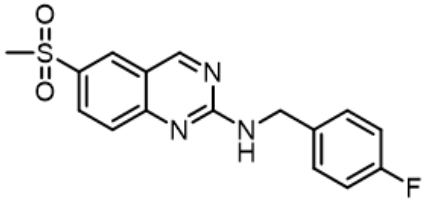
1 n=0, R_1= F, R_2= Me	**13** n=0, R_1= 3,5-dimethoxy, R_2= Me	**25** n=1, R_1= OMe, R_2= Me
2 n=0, R_1= F, R_2= Et	**14** n=0, R_1= 3,5-dimethoxy, R_2= Me	**26** n=1, R_1= OMe, R_2= Et
3 n=0, R_1= CF_3, R_2= Me	**15** n=1, R_1= F, R_2= Me	**27** n=1, R_1= 3,5-dimethoxy, R_2= Me
4 n=0, R_1= CF_3, R_2= Et	**16** n=1, R_1= F, R_2= Et	**28** n=1, R_1= 3,5-dimethoxy, R_2= Et
5 n=0, R_1= OCH_2O, R_2= Me	**17** n=1, R_1= CF_3, R_2= Me	**29** n=1, R_1= Pyridine, R_2= Me
6 n=0, R_1= OCH_2O, R_2= Et	**18** n=1, R_1= CF_3, R_2= Et	**30** n=1, R_1= Pyridine, R_2= Et
7 n=0, R_1= OH, R_2= Me	**19** n=1, R_1= OCH_2O, R_2= Et	**31** n=2, R_1= Indole, R_2= Me
8 n=0, R_1= OH, R_2= Et	**20** n=1, R_1= OCH_2O, R_2= Et	**32** n=2, R_1= Indole, R_2= Et
9 n=0, R_1= $C(CH_3)3$, R_2= Me	**21** n=1, R_1= OH, R_2= Me	**67** n=1, R_1= F, R_2= Me
10 n=0, R_1= $C(CH_3)3$, R_2= Et	**22** n=1, R_1= OH, R_2= Et	**68** n=1, R_1= F, R_2= Et
11 n=0, R_1= OMe, R_2= Me	**23** n=1, R_1= $C(CH_3)3$, R_2= Me	**69** n=1, R_1= CF_3, R_2= Me
12 n=0, R_1= OMe, R_2= Et	**24** n=1, R_1= $C(CH_3)3$, R_2= Et	**70** n=1, R_1= CF_3, R_2= Et

Figure 2.5: Scheme 2: Routes employed towards synthesis of quinoline analogues and library of molecules synthesized. Reagents and conditions. (i) Cinnamoyl chloride, Pyridine, DMAP, DCM, 0 °C- RT, 3-4 h (ii) $AlCl_3$, DMA, Reflux, 4-5 h (iii) $POCl_3$, 105 °C, 3h (iv) Ethanol, 150 °C (24-48h) (v) RSO_2Na, CuI, L-Proline, K_2CO_3, DMSO, 130 °C, 12h.

The detailed experimental procedures are discussed in the experimental section (4.1.2). All the final compounds are fully characterized by ^{1}H-NMR, ^{13}C-NMR, LCMS and purity was checked using reverse phase HPLC (>95 %). Characterization data of lead compounds **15** (SG-02), **18** (SG-39), and **29** (SG-60) are as follows. (Figure 2.6-2.17)

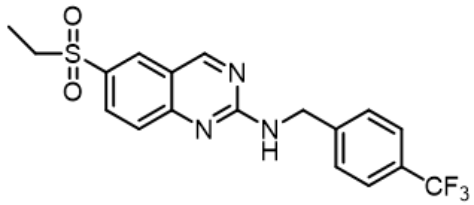
N-(4-fluorobenzyl)-6-(methylsulfonyl)quinazolin-2-amine, cpd 15 (SG-02):

Pale yellow solid, (114 mg, 57%), **^{1}H NMR (DMSO-d_6, 500 MHz) δ_H:** 9.28 (s, 1H), 8.45 (t, *J*=3.75 Hz, 1H), 8.39 (d, *J*=2.5 Hz, 1H), 8.03 (dd, *J* = 11.3, 2.8 Hz, 1H), 7.55 (d, *J* = 11 Hz, 1H), 7.38 (t, *J* = 8.25 Hz, 2H), 7.09 (m, 2H), 4.57 (d, *J* = 7 Hz, 2H), 3.19 (s, 3H); **^{13}C NMR (DMSO-d_6, 125 MHz) δ_C:** 164.2, 161.6 (d, *J* = 241.1 Hz), 136.1, 133.9, 131.3, 129.8 (d, *J* = 7.7Hz), 129.4, 126.6, 118.9, 115.4 (d, *J* = 21.1 Hz), 44.1, 43.8; LCMS calculated for $C_{16}H_{15}FN_3O_2S$ $[M+H]^+$, 332.0869, found 332.0908; HPLC purity observed was 96.9%.



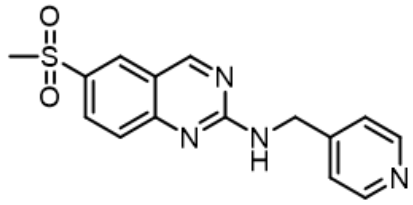
6-(ethylsulfonyl)-N-(4-(trifluoromethyl)benzyl)quinazolin-2-amine, cpd 18 (SG-39):

Pale yellow solid, (115 mg, 55.5 % yield), **^{1}H NMR (DMSO-d_6, 500 MHz) δ_H:** 9.37 (s, 1H), 8.63 (t, *J*= 6 Hz, 1H), 8.43 (d, *J*= 2 Hz, 1H), 8.01 (d, *J* = 10.5, 1H), 7.69 (d, *J*= 8.5 Hz, 2H), 7.59 (m, 3H), 4.73 (d, *J*= 6 Hz, 2H), 3.32 (q, *J*= 7.0 Hz, 2H), 1.15 (d, *J*= 7.5 Hz ,3H) ; **^{13}C NMR (DMSO-d_6, 125 MHz) δ_C:** 164.4, 161.1, 154.2, 144.9, 131.9, 131.5, 130.6, 128.4, 128.0-127.9 (m), 127.7-125.9 (m), 126.7, 125.6 (q, *J* = 4.2 Hz), 123.7, 119.0, 49.7, 44.2, 7.8; LCMS calculated for $C_{18}H_{17}F_3N_3O_2S$ $[M+H]^+$, 396.0994, found 396.0975; HPLC purity observed was 98.9%.



6-(methylsulfonyl)-N-(pyridin-4-ylmethyl)quinazolin-2-amine, (cpd 29), SG-60:

Light yellow solid (110 mg, 55 % yield), **^{1}H NMR (DMSO-d_6, 500 MHz) δ_H:** 9.36 (s, 1H), 8.57(t, *J* = 9.0 Hz, 1H), 8.47 (d, *J* = 5.0 Hz, 2H), 8.44 (d, *J* = 2.0 Hz, 1H), 8.05 (d, *J*= 8.5 Hz, 1H), 7.55 (d, *J*= 9.0 Hz, 1H), 7.34 (d, *J*= 4.5 Hz, 2H), 4.65 (d, *J*= 6.0 Hz, 2H), 3.32 (s, 3H) ; **^{13}C NMR (DMSO-d_6, 125 MHz) δ_C :**164.4, 161.1, 154.0, 149.9, 149.0, 134.0, 131.3, 129.4, 126.6, 122.6, 118.9, 44.1, 43.6; LCMS calculated for $C_{15}H_{15}N_4O_2S$ $[M+H]^+$, 315.0916, found 315.0912; HPLC purity observed was 99.0%.



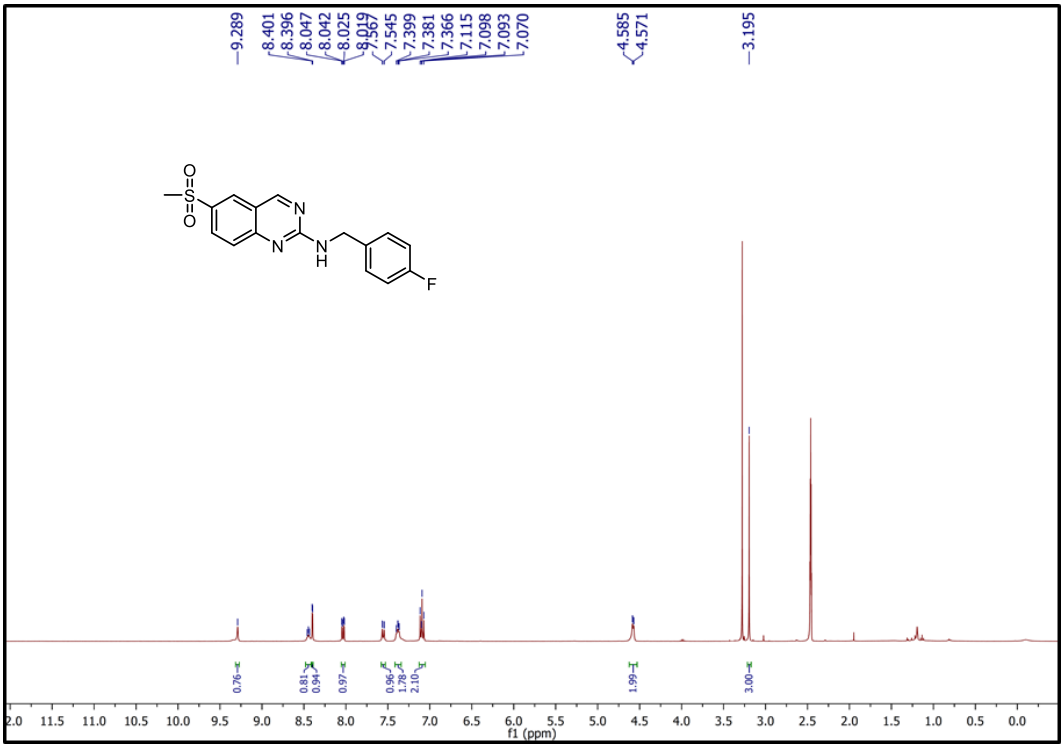


Figure 2.6: [1]HNMR spectra of **cpd 15 (SG-02)** (500 MHz, DMSO-d6)

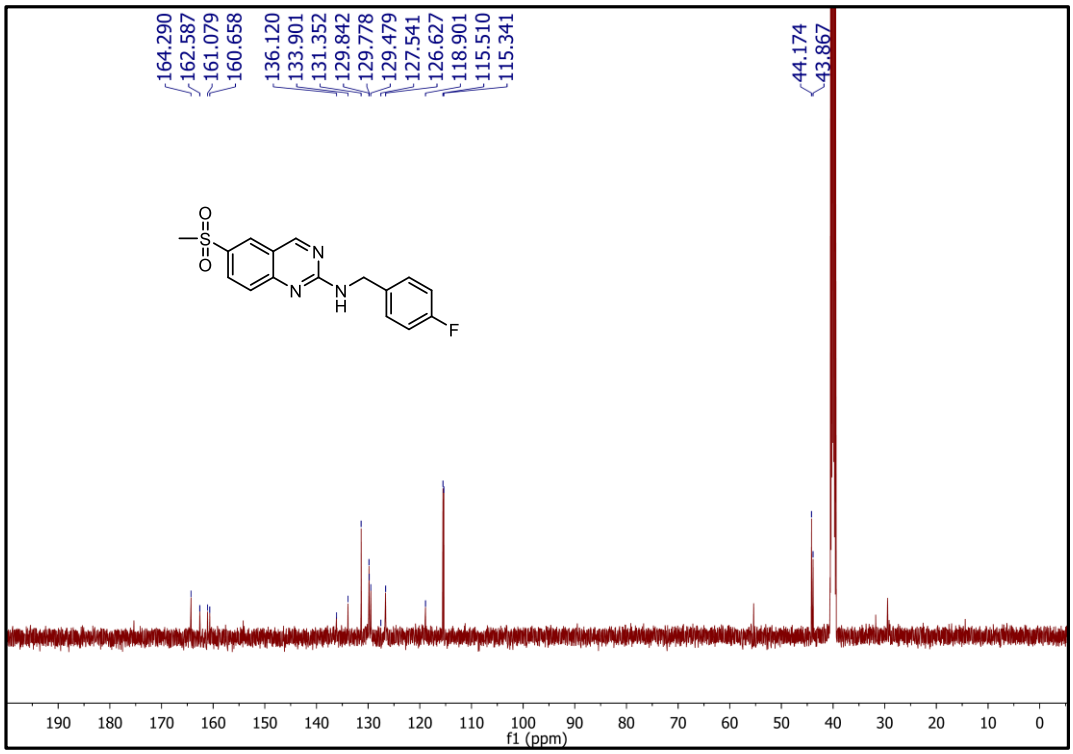
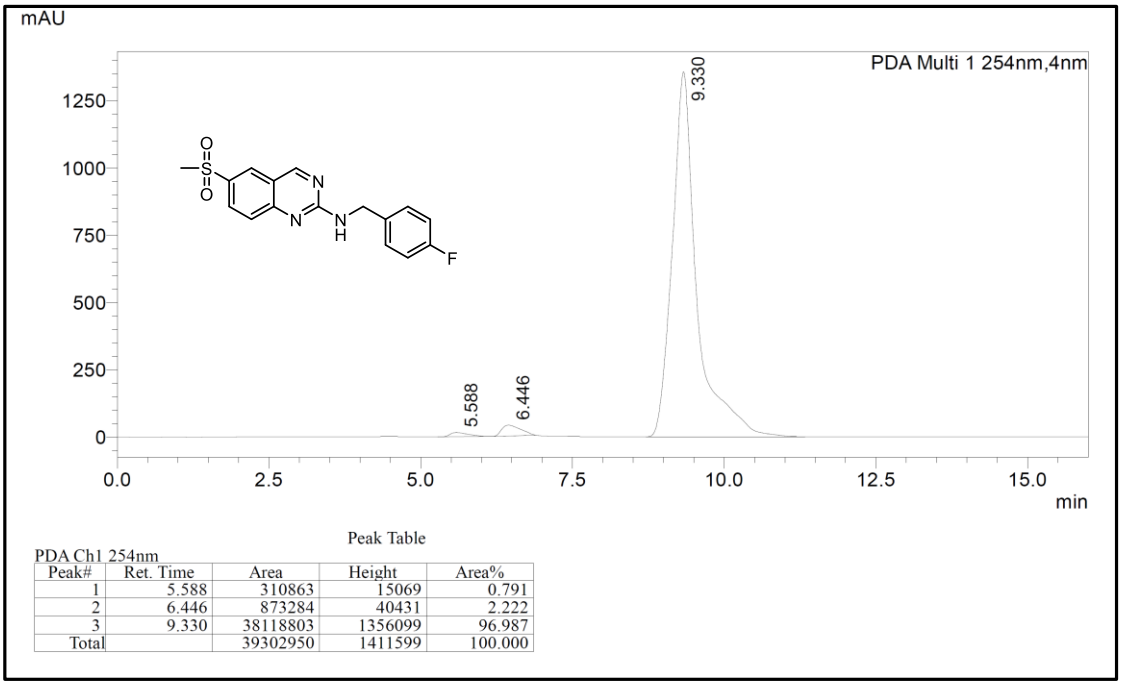


Figure 2.7: [13]CNMR spectra of **cpd 15 (SG-02)** (125 MHz, DMSO-d6)



Peak Table

PDA Ch1 254nm

Peak#	Ret. Time	Area	Height	Area%
1	5.588	310863	15069	0.791
2	6.446	873284	40431	2.222
3	9.330	38118803	1356099	96.987
Total		39302950	1411599	100.000

Figure 2.8: HPLC chromatogram of cpd 15 (SG-02)

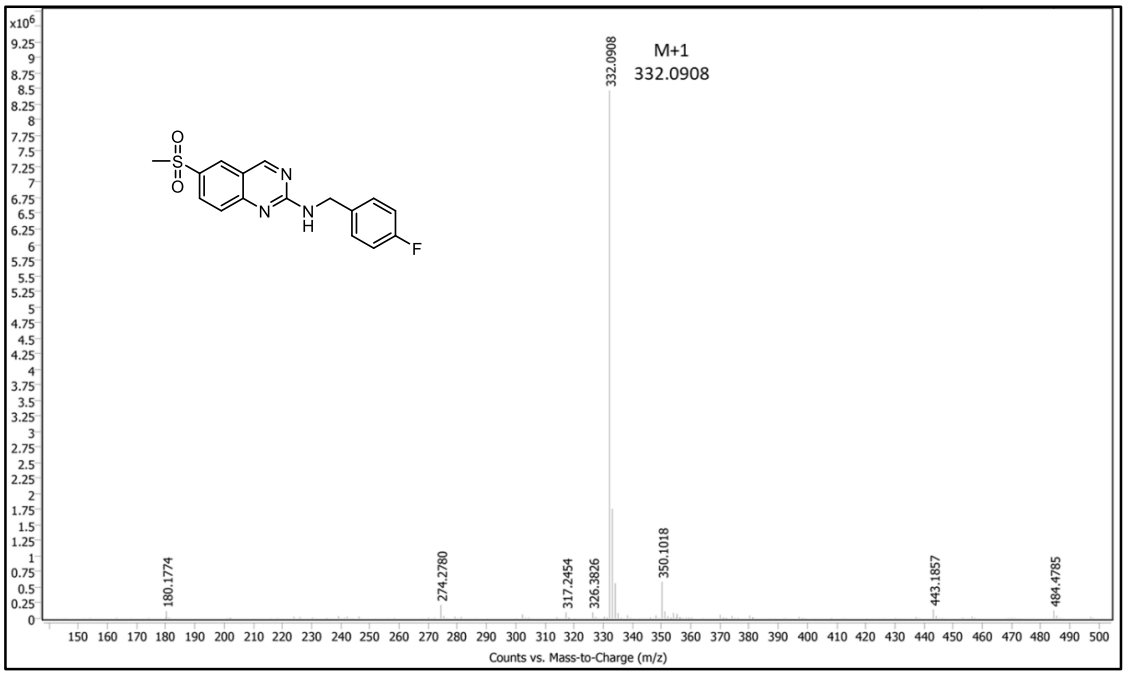


Figure 2.9: ESI-MS spectra of cpd 15 (SG-02)

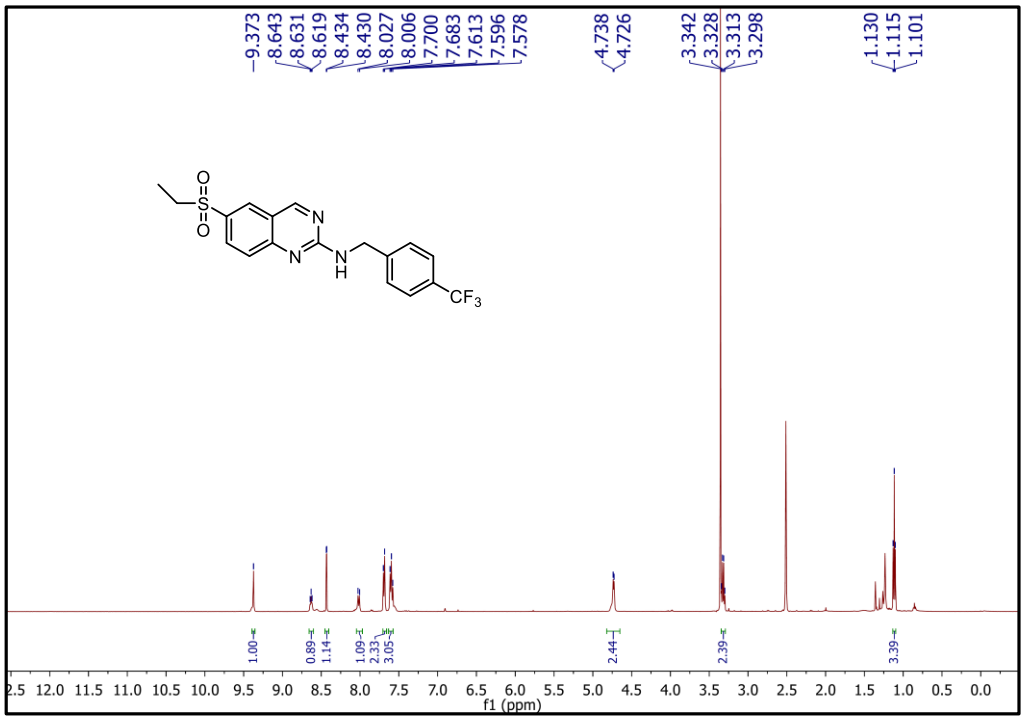


Figure 2.10: [1]HNMR spectra of **cpd 18 (SG-39)** (500 MHz, DMSO-d6)

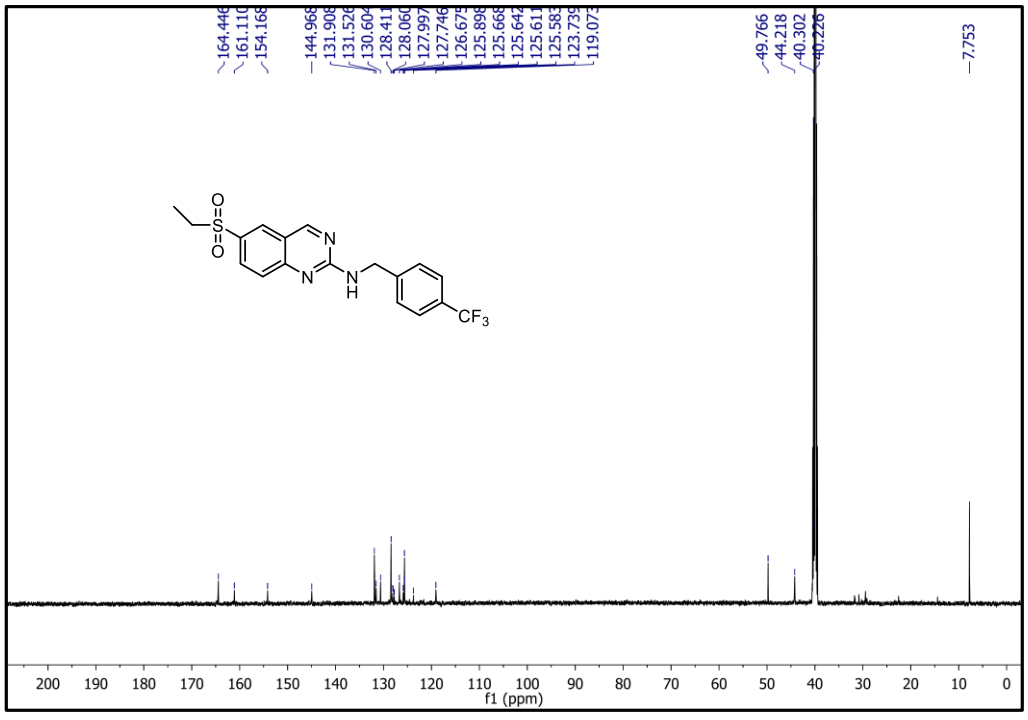
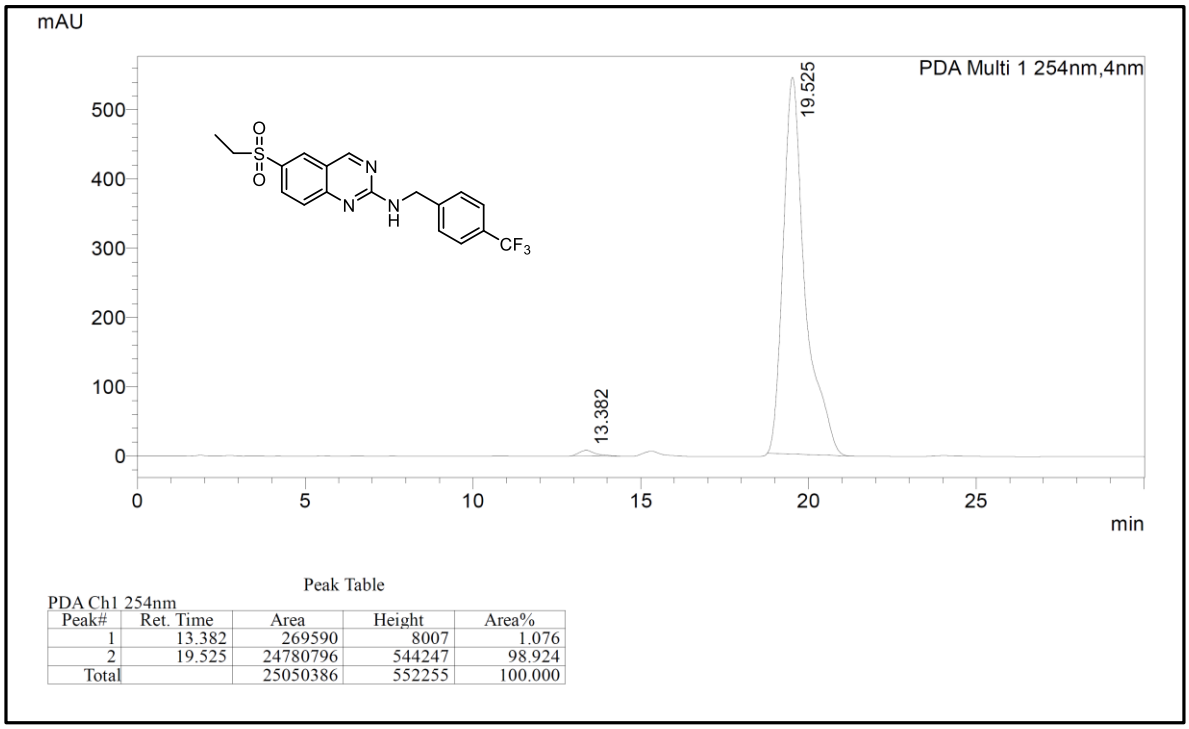


Figure 2.11: [13]CNMR spectra of **cpd 18 (SG-39)** (125 MHz, DMSO-d6)



Peak Table

PDA Ch1 254nm

Peak#	Ret. Time	Area	Height	Area%
1	13.382	269590	8007	1.076
2	19.525	24780796	544247	98.924
Total		25050386	552255	100.000

Figure 2.12: HPLC chromatogram of cpd 15 (SG-02)

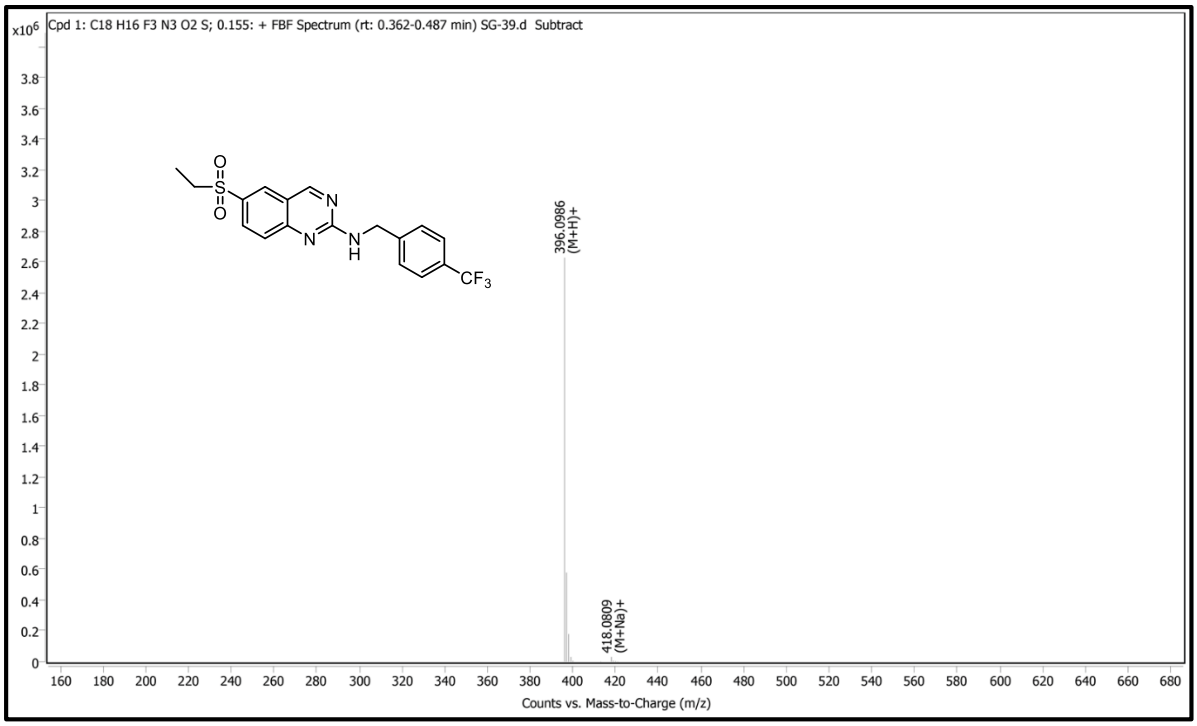


Figure 2.13: ESI-MS spectra of cpd 18 (SG-39)

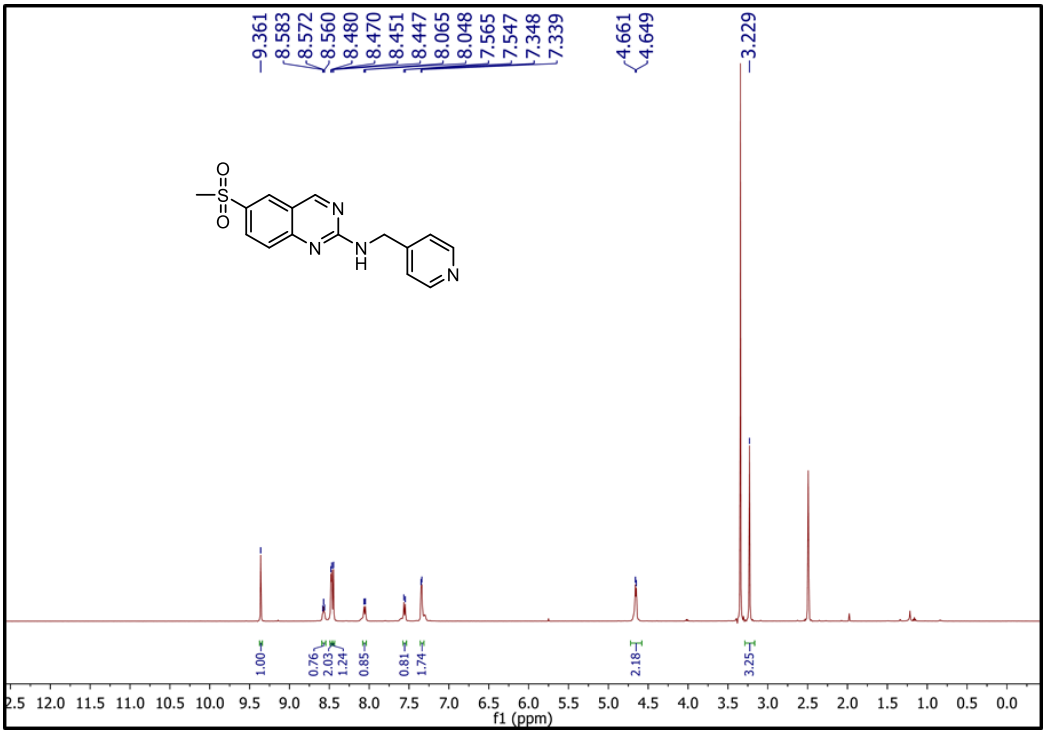


Figure 2.14: [1]HNMR spectra of **cpd 29 (SG-60)** (500 MHz, DMSO-d6)

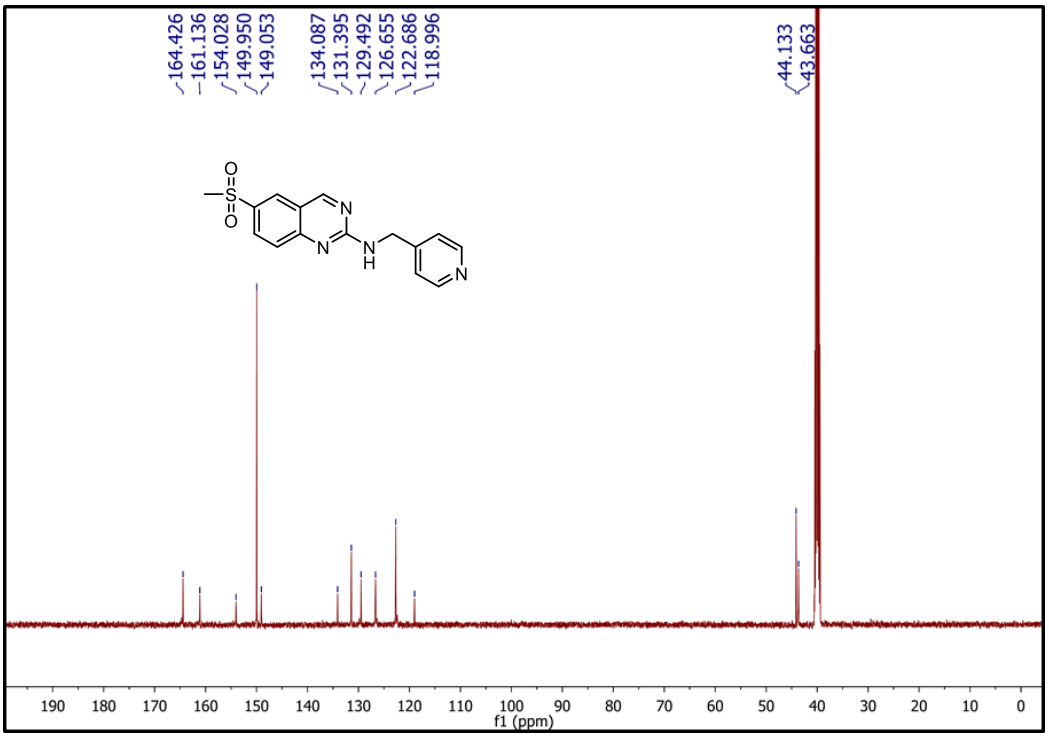
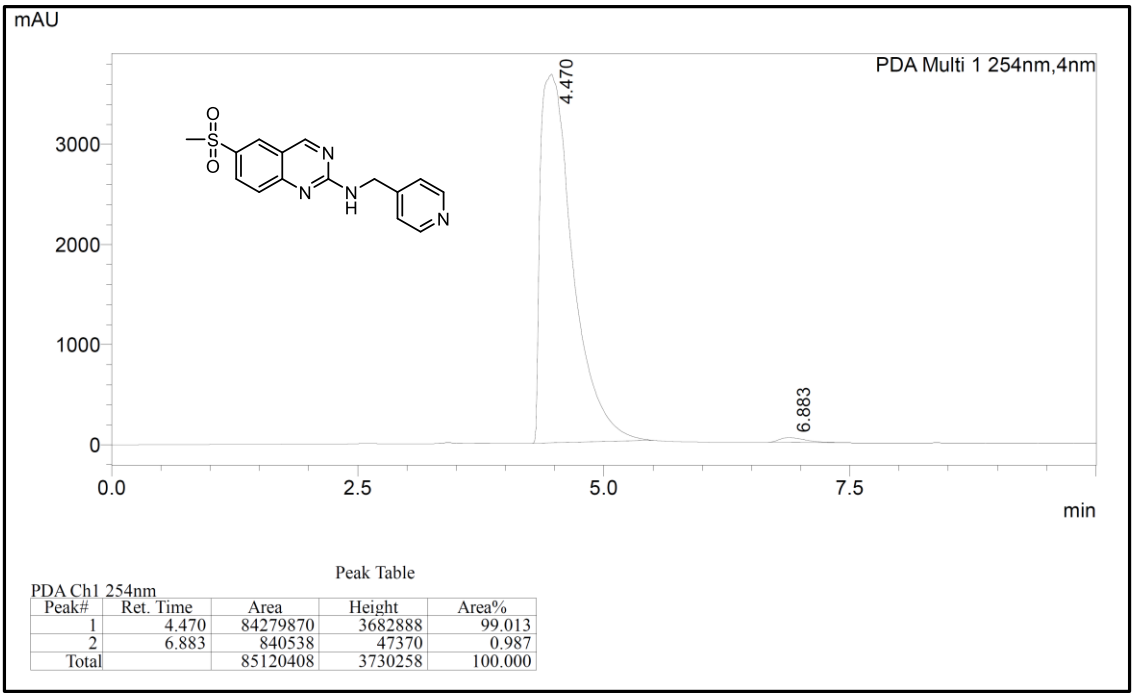


Figure 2.15: [13]CNMR spectra of **cpd 29 (SG-60)** (125 MHz, DMSO-d6)



Peak Table

PDA Ch1 254nm

Peak#	Ret. Time	Area	Height	Area%
1	4.470	84279870	3682888	99.013
2	6.883	840538	47370	0.987
Total		85120408	3730258	100.000

Figure 2.16: HPLC chromatogram of cpd 29 (SG-60)

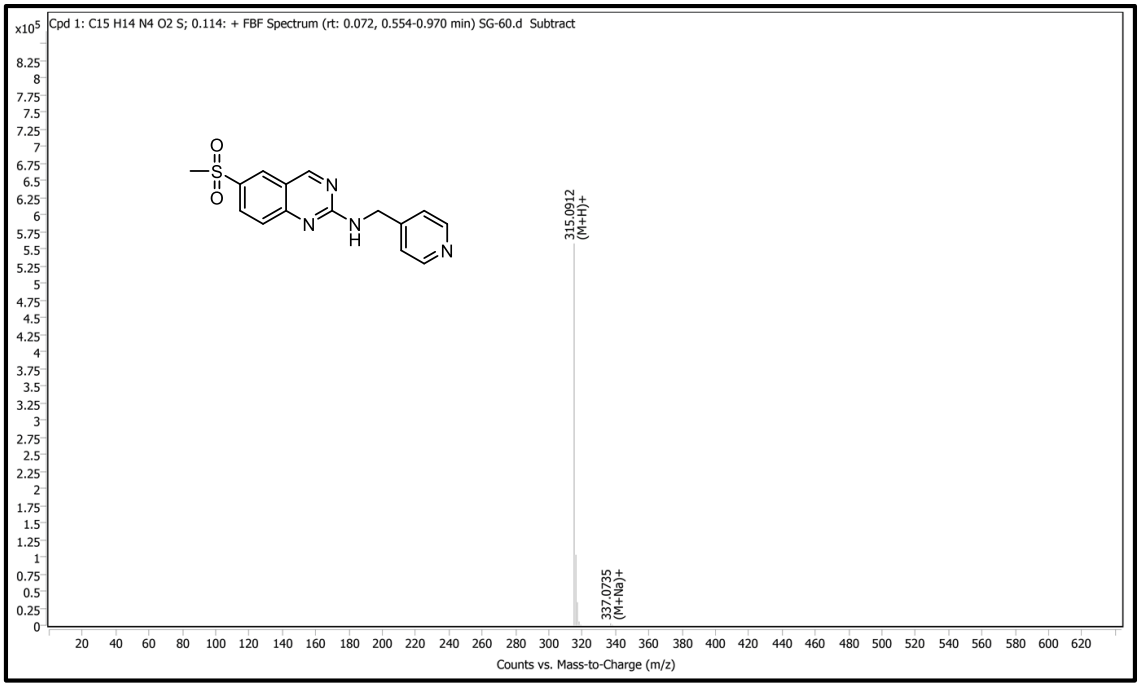


Figure 2.17: ESI-MS spectra of cpd 29 (SG-60)

2.3.4 Screening of Molecular Library by High-throughput In-Cell ELISA Technique

In-Cell ELISA is a sensitive and quantitative technique that allows the measurement of intracellular protein without the requirements of cell lysis. Herein, it was employed to screen the synthesized molecular library. To assess the potency of drug candidates in the nanomolar range and determine the optimal concentration at which the utrophin expression is high, we selected four molecules (**13**, **16**, **17**, and **32**) from our library, with different R_1, R_2 groups, and varying core scaffolds. C2C12 myoblast cells were treated with these molecules at three different concentrations (200 nM, 400 nM and 800 nM) for 72 hr, and it was observed that at 800 nM concentration utrophin expression was significantly higher (Figure 2.18 A-D).

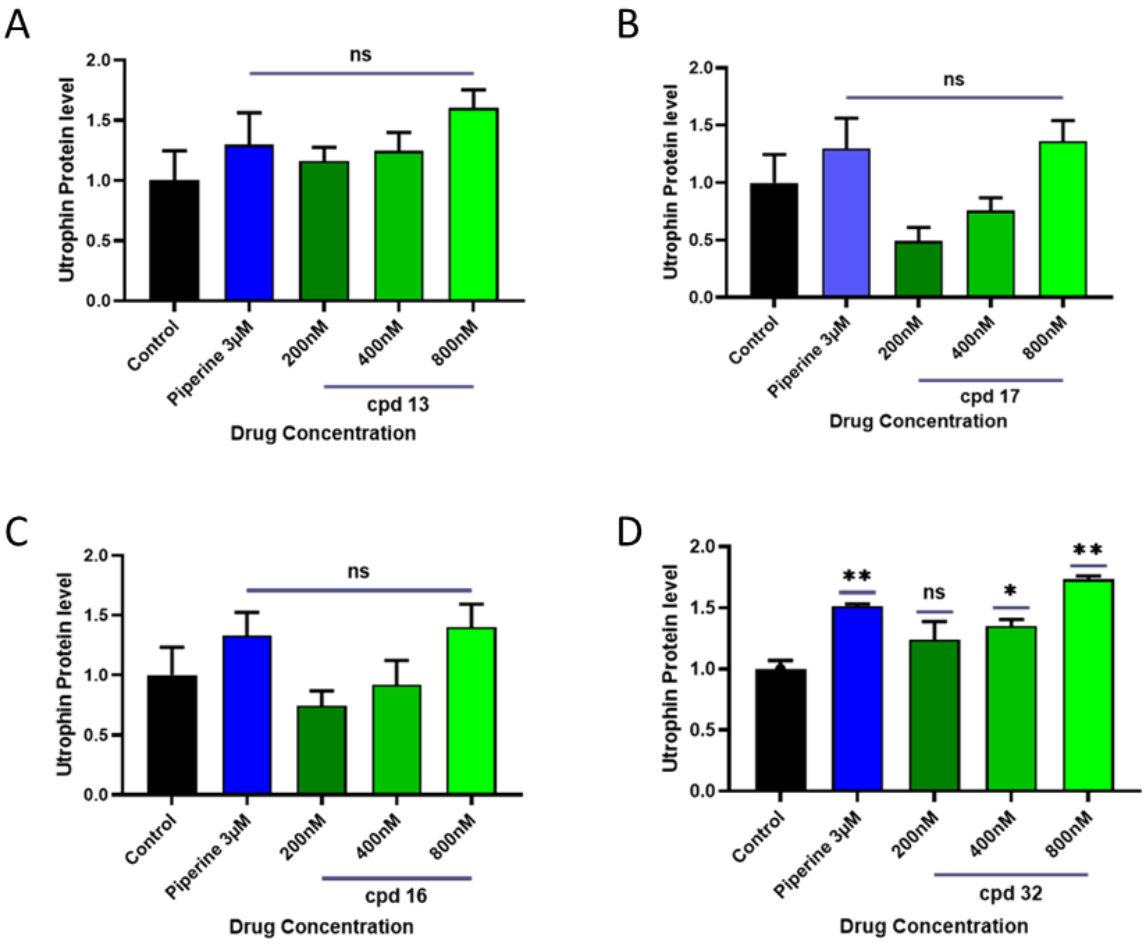
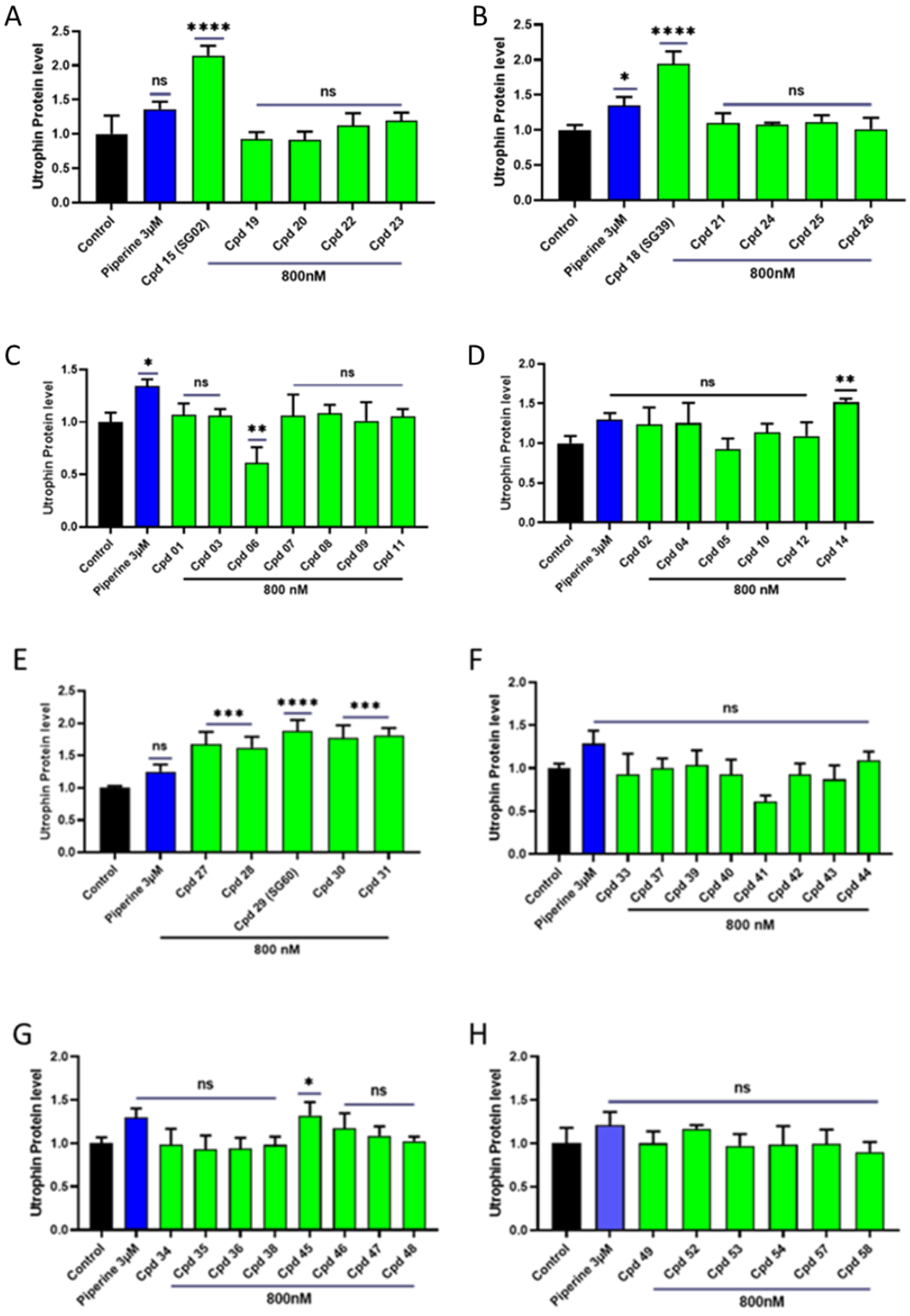


Figure 2.18: (A-D) In-Cell ELISA Data for Determination of Optimal Screening Concentration for cpd 13, 16, 17, 32. In all data sets, significance was calculated using one-way ANOVA, *p< 0.05, **p<0.01

So, for further screening of our small molecules library, we selected 800 nM as the optimum concentration (Figure 2.19 A-K). Herein, piperine was chosen as our positive control.[20] The **15** (SG-02), **18** (SG-39), and **29** (SG-60) displayed the highest utrophin upregulation of 2.14, 1.94, and 1.88 folds among all the 70 molecules screened at 800 nM concentration in comparison to the positive control piperine, which demonstrated 1.3-fold increase in utrophin protein at a concentration of 3

µM (Figure 2.19 A, B &E). These molecules were identified as lead candidates and were selected for further validation of their role as utrophin up-regulators.



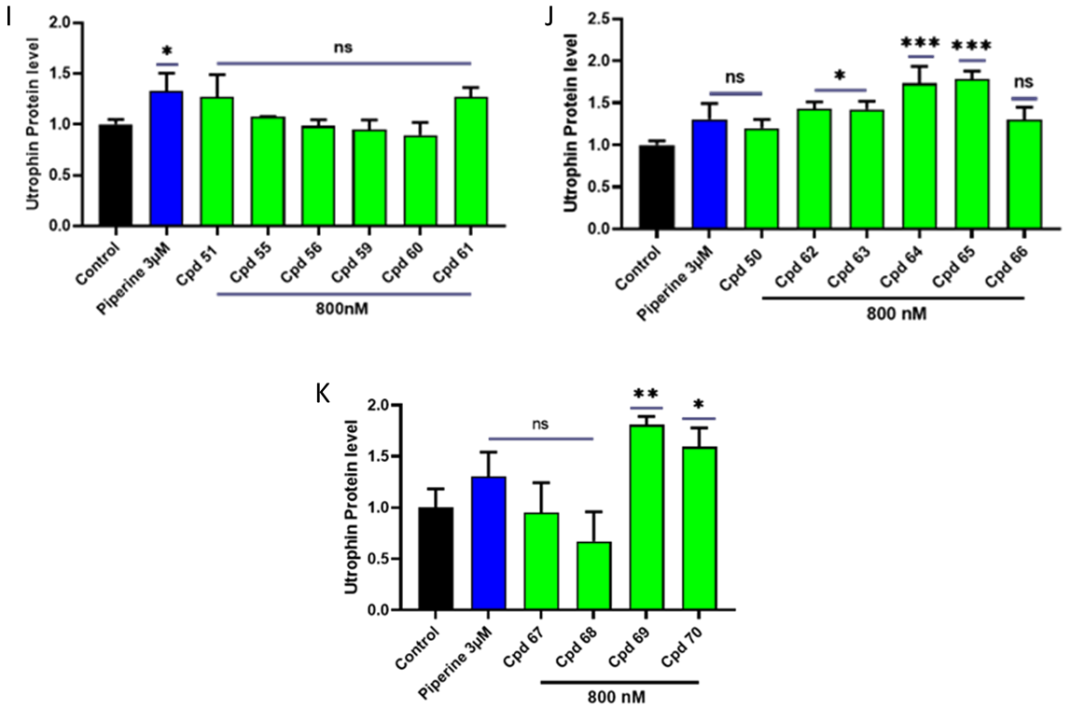


Figure 2.19: (A-K) In-Cell ELISA Data for Screening of the Molecular Library at 800 nM. In all data sets, significance was calculated using one-way ANOVA, *p< 0.05, **p<0.01, ***p<0.001, ****p<0.0001.

2.3.5 Cellular Cytotoxicity

Cytotoxicity of the quinazoline and quinoline based small molecules was measured by the MTT (3-[4,5-dimethylthiazol-2-yl]-2,5 diphenyl tetrazolium bromide) assay after treatment of C2C12 myoblast cells with each molecule at varied concentrations (0.78, 1.56, 3.125, 6.25, 12.5, 25, 50, 100 µM) for 24 h.

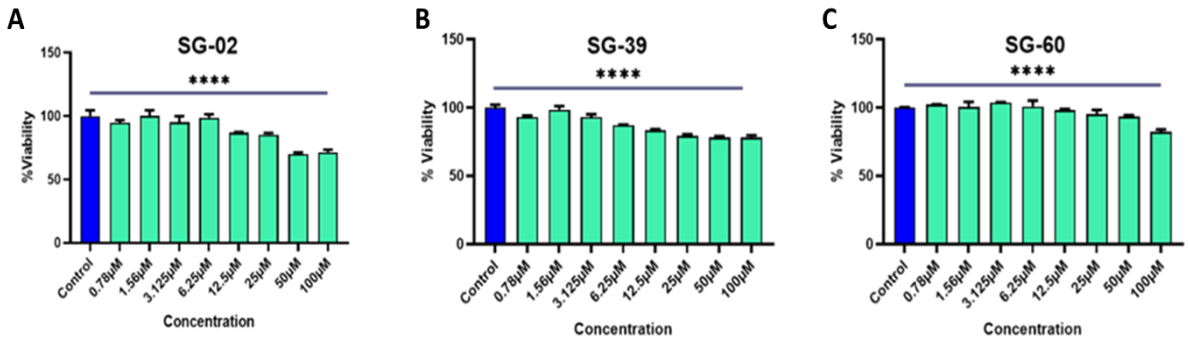


Figure 2.20: (A-C) Cell survival percentage after treatment of C2C12 myoblast cells with the three lead molecules (SG-02, SG-39, and SG-60) identified in an increasing gradient of doses (3.125-100 µM) for 24 h, n=3. In all data sets, significance was calculated using one-way ANOVA, ****p<0.0001.

The obtained results, as illustrated in Figure 2.20 for lead molecules, (SG-02, SG-39, and SG-60) distinctly revealed that all the administered molecules exhibited negligible toxicity even

at higher concentrations. These findings suggest that the lead molecules possess a favourable safety profile, particularly at therapeutic concentrations, making them promising candidates for further development.

2.3.6 Structure Activity Relationship

All the molecules synthesized herein were screened through high throughput In-Cell ELISA technique. Seeking to establish the structural variation required for activity as depicted in Figure 2.21, we investigated the (i) basic core scaffold, which varies between quinoline and quinazoline motif. (ii) variation of the active substituents appended to the C-2 position of the basic core scaffolds. (iii) aqueous soluble motif on the C-6 position of the core scaffolds with variations encompassing both ethyl and methyl substitutions of sulfonyl. (iv) a positional variation of the aqueous soluble motif was carried out for the lead molecules identified, **15** (SG-02) and **18** (SG-39), by shifting it from the C-6 to the C-7 position of the quinazoline scaffold.

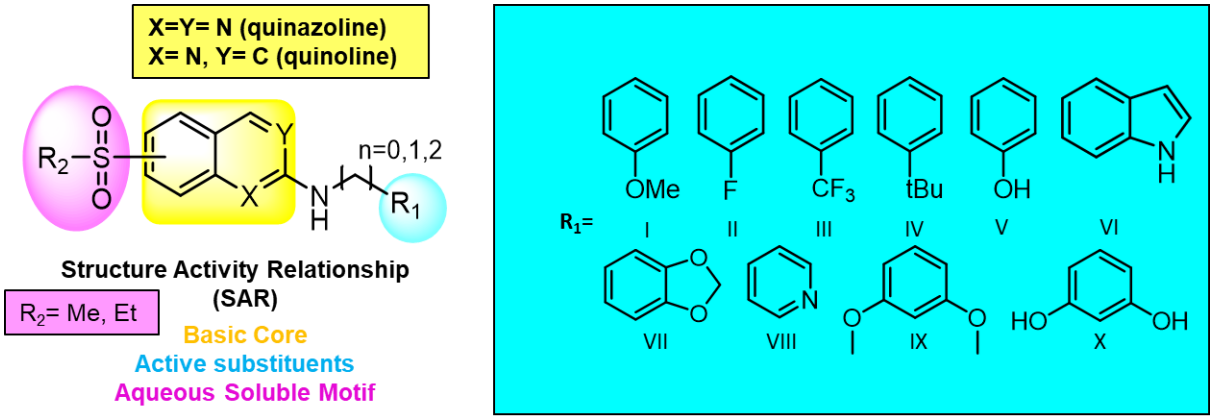
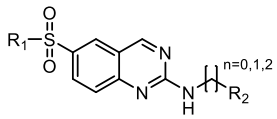


Figure 2.21: Core scaffold structures and key regions of interest for structure-activity relationships, illustrating the ligand library and variations in aqueous-soluble motifs.

The rationale behind selecting the quinoline and quinazoline scaffolds has already been discussed in the previous section (2.1). In order to optimize the basic core scaffold and transform it into an advanced functional motif, we focused on incorporating active substituents at the C-2 position of both quinoline and quinazoline cores. Herein, the choice of ligands that are categorized as active substituents are inspired by relevant literature studies. For instance, the preference for ligands incorporating halogen atoms at the para position (II, III) and those involving heteroatom substitution (VIII) draws inspiration from compounds recognized for their ability to enhance utrophin expression and ensure metabolic stability.[18] Whereas, the incorporation of the V, VI, and VII motifs drew inspiration from both natural compounds, such as piperine and resveratrol,[20] and synthetic utrophin Upregulators like GNF-351.[26] Additionally, to investigate the activity of hydrophobic motifs, t-butyl (IV) and -O-Me (I) substitutions were introduced. Furthermore, to enhance oral bioavailability, an aqueous soluble motif was introduced at the C-6 position of the core structure, with variations in both ethyl and methyl substitutions of sulfonyl.



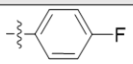
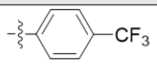
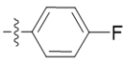
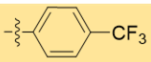
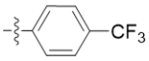
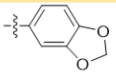
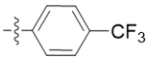
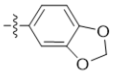
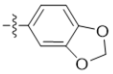
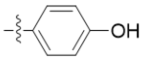
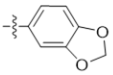
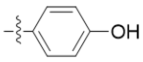
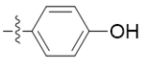
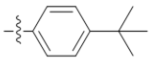
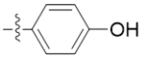
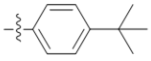
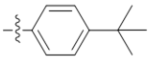
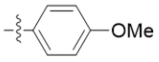
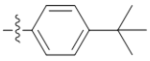
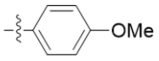
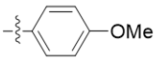
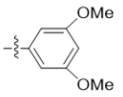
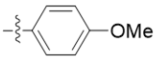
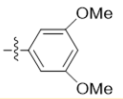
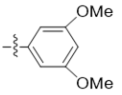
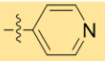
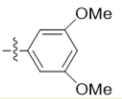
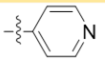
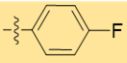
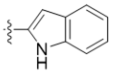
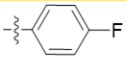
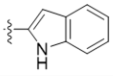
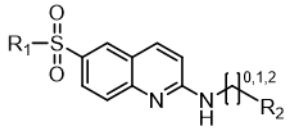
cpd	n	R_1	R_2	Utrophin upregulation via In-Cell ELISA (0.8µM)	cpd	n	R_1	R_2	Utrophin upregulation via In-Cell ELISA (0.8µM)
1	0	Me		1.06	**17**	1	Me		1.27
2	0	Et		1.23	**18 (SG-39)**	1	Et		1.93
3	0	Me		1.06	**19**	1	Me		0.92
4	0	Et		1.25	**20**	1	Et		0.91
5	0	Me		0.92	**21**	1	Me		1.09
6	0	Et		0.60	**22**	1	Et		1.12
7	0	Me		1.06	**23**	1	Me		1.19
8	0	Et		1.08	**24**	1	Et		1.07
9	0	Me		1.01	**25**	1	Me		1.11
10	0	Et		1.13	**26**	1	Et		1.01
11	0	Me		1.05	**27**	1	Me		1.67
12	0	Et		1.09	**28**	1	Et		1.62
13	0	Me		1.60	**29 (SG-60)**	1	Me		1.88
14	0	Et		1.52	**30**	1	Et		1.77
15 (SG-02)	1	Me		2.14	**31**	2	Me		1.81
16	1	Et		1.40	**32 (SG-51)**	2	Et		1.73

Table 2.1: Structure-activity relationships with basic quinazoline scaffold and varying R_1 and R_2 substitution with variable chain length of n = 0,1,2. Each data set represent the average of three replicates. Here cpd signifies for compounds.

Our efforts to develop a novel utrophin modulator, incorporating modifications in three distinct variables and elucidating the structure-activity relationships of the resulting molecules arising from structural changes, have been represented in Tables 2.1 and 2.2. Additionally, Table 2.3 elucidates the intricate structure-activity relationships existing within the regioisomers of the lead molecules, SG-02 and SG-39. To summarize the findings obtained from the high-throughput screening of all synthesized molecules and to establish a minimum structure-activity relationship, several significant observations were made. Firstly, our observations revealed that the quinazoline core structure generally exhibits superior utrophin upregulation compared to the quinoline core (Tables 2.1 illustrate quinazoline compounds with augmented efficacy in contrast to their quinoline counterparts indicated in Tables 2.2), which implies that the presence of two nitrogen atoms on the core scaffold benefits or enhances the utrophin upregulation. Notably, a deviation from this trend was observed with the VII ligand, where **6** and **19** exhibited relatively diminished utrophin upregulation compared to their quinoline analogues **37** and **54**, which displayed a distinct and reversed structure-activity relationship.

Secondly, while examining substitutions at the C-2 position of the core scaffold with library amines, it was observed that compounds containing chain length of n=1, 2 exhibited more favourable profiles in terms of utrophin upregulation as compared to those with direct -NH substitution (n=0). This observation was supported by the higher utrophin fold change for **15** to **32** in Table 2.1 (quinazoline scaffold) and **49** to **66** in Table 2.2 (quinoline scaffold) as compared to **1** to **14** in Table 2.1 and **33** to **48** in Table 2.2. In this context, we made another noteworthy observation by comparing the effects of direct –NH substitution (n=0) with those containing chain length of n=1, 2 in appending active substituents to the core scaffold. With direct -NH substitution (n=0), substituents attached at C-2 position showed similar utrophin upregulation profiles as shown in Table 2.1 (**1** to **12**) and Table 2.2 (**33** to **48**), across all ligands except for ligand IX, which displayed a distinct and promising utrophin upregulation pattern (**13**, **14**, **45**, and **46**). However, when utilizing the chain lengths n=1, 2 for attaching active substituents, significant variations in the utrophin upregulation profile were observed, depending on the specific functional groups chosen from the library amines, as depicted in Table 2.1 (**15** to **32**) and Table 2.2 (**49** to **66**). This finding highlights the importance of the bridge with chain length n=1, 2 in modulating the activity and efficacy of the attached substituents for utrophin upregulation. Next, in our effort to identify the effectiveness of different active substituents linked at the C-2 position to the core structure, we have observed that ligands such as (II, III, VI, VIII, and IX) group exhibited the most pronounced utrophin upregulation profile and displayed notable variability.

However, we did not observe any distinct ascending or descending trend in activity among these ligands, as their activity patterns are subject to the influence of different other variations, such as alterations in the basic core scaffold (quinazoline and quinoline), and in the aqueous soluble motif. In contrast, ligands such as I, IV, V, and VII exhibited comparatively lower and nearly equivalent levels of utrophin upregulation. Interestingly, increasing the methoxy substitutions from 4-OMe (ligand I) to 3,5-dimethoxy (ligand IX) has enhanced the utrophin upregulation profile across both quinoline and quinazoline scaffolds. As for quinazoline scaffold **13**, **14**, **27** and **28** containing the 3,5 dimethoxy group displayed a more significant fold change compared to **11**, **12**, **25**, and **26** with 4-OMe substitution.



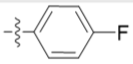
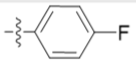
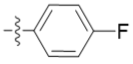
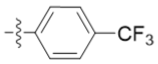
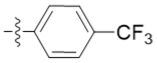
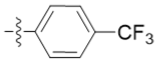
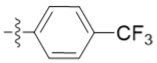
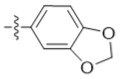
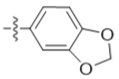
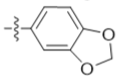
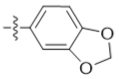
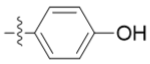
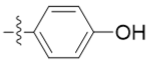
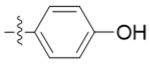
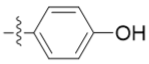
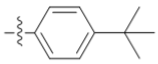
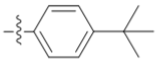
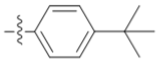
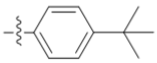
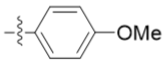
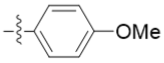
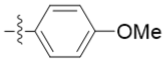
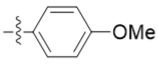
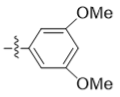
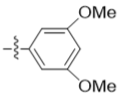
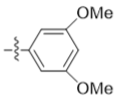
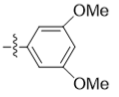
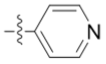
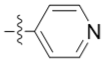
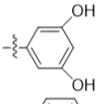
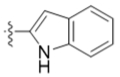
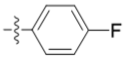
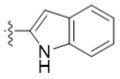
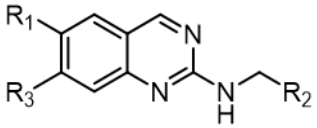
cpd	n	R_1	R_2	Utrophin upregulation via In-Cell ELISA (0.8µM)	cpd	n	R_1	R_2	Utrophin upregulation via In-Cell ELISA (0.8µM)
33	0	Me		0.93	**50**	1	-Et		1.20
34	0	Et		0.98	**51**	1	-Me		1.27
35	0	Me		0.93	**52**	1	-Et		1.16
36	0	Et		0.94	**53**	1	-Me		0.97
37	0	Me		1.00	**54**	1	-Et		0.98
38	0	Et		0.98	**55**	1	-Me		1.07
39	0	Me		1.03	**56**	1	-Et		0.98
40	0	Et		0.93	**57**	1	-Me		0.99
41	0	Me		0.61	**58**	1	-Et		0.90
42	0	Et		0.93	**59**	1	-Me		0.94
43	0	Me		0.87	**60**	1	-Et		0.89
44	0	Et		1.09	**61**	1	-Me		1.26
45	0	Me		1.32	**62**	1	-Et		1.42
46	0	Et		1.17	**63**	1	-Me		1.42
47	0	Me		1.08	**64 (SG-56)**	1	-Et		1.73
48	0	Et		1.02	**65 (SG-55)**	2	-Me		1.78
49	1	Me		1.00	**66**	2	-Et		1.30

Table 2.2: Structure-activity relationships with basic quinoline scaffold and varying R1 and R2 substitution with variable chain length of n = 0, 1, 2. Each data set represent the average of three replicates. Here cpd signifies for compounds.

Similarly, for quinoline core scaffolds **45**, **46**, **61**, and **62** exhibited comparatively improved fold changes compared to **43**, **44**, **59**, and **60**. In contrast to the aforementioned observations, the increase of hydroxy group substitution from para hydroxy (ligand V) to 3, 5 dihydroxy (ligand X) exhibited almost identical utrophin expression upon evaluation with the quinoline core scaffold (exemplified by **39** and **40** containing para hydroxy group compared to **47** and **48** having 3, 5 dihydroxy group as illustrated in Table 2.2), thus no further synthesis and analysis involving ligand X was conducted. Whereas variation of the aqueous soluble motif R_1 from methyl to ethyl substitution and vice versa does not display any consistent trend in the screening studies. This suggests that both cohorts are engaged in activity, and their activity patterns are influenced by variations in other parameters. Lastly, to determine the influence of position for the aqueous soluble group on the basic core structure, if any, on the utrophin upregulation profile, we have synthesized the regioisomers of two lead molecules identified SG-02 and SG-39. This was attained by repositioning both -$MeSO_2$ and -$EtSO_2$ groups from C-6 to C-7 position of the core structure.



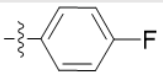
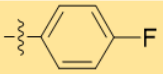
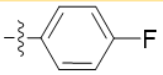
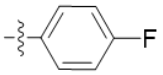
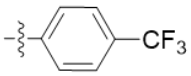
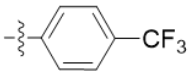
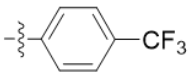
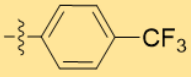
Compound (cpd)	R_1	R_2	R_3	Utrophin upregulation via In-Cell ELISA (0.8µM)
67	-H			0.95
15 (SG-02)			-H	2.14
68	-H			0.67
16			-H	1.40
69	-H			1.80
17			-H	1.27
70	-H			1.51
18 (SG-39)			-H	1.93

Table 2.3: Structure-activity relationship analyzing regioisomers of aqueous soluble motif for lead molecule SG-02 and SG-39. Each data set represent the average of three replicates. Here cpd signifies for compounds.

Following analysis of the data concerning these regioisomers, it was observed that the presence of the aqueous soluble motif in the C-6 position (**15**, **16**, **17**, and **18**) resulted in a more favourable outcome compared to the substitution at the C-7 position (**67**, **68**, **69**, and **70**) of the quinazoline scaffold. These findings provide insights into the significance of a specific position of the aqueous soluble group in augmenting utrophin upregulation.

Overall, our comprehensive analysis provides insights into the structural modifications necessary for effective utrophin modulation and sheds light on the influence of different variables on utrophin upregulation. In this study, our objective was to investigate the impact of structural variation on the desired outcomes. The collective results obtained offer compelling evidence supporting the efficacy and rationale of our design approach. Notably, through a rigorous high-throughput In-Cell ELISA screening technique performed, we identified three hit molecules 15 (SG-02), 18 (SG-39), and 29 (SG-60) from a library of seventy compounds synthesized. These hit molecules displayed significant potential in terms of utrophin upregulation. Subsequently, the selected hit molecules underwent a comprehensive evaluation to assess their viability as leads to gain deeper mechanistic insights.

2.3.7 qRT-PCR and Western Blot of Hit Molecules Identified

For further assessing the role of the lead molecules as utrophin up-regulators, qRT-PCR was performed for all three lead molecules SG-02, SG-39 and SG-60 after treating the C2C12 myoblast cell line with 800 nM concentration relative to positive control piperine at 3 µM for 72 hr.

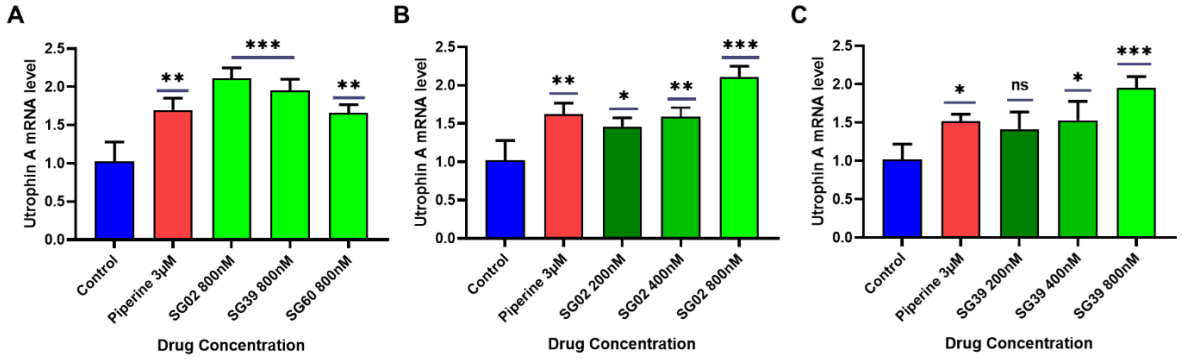


Figure 2.22: qRT-PCR assay. (A) Utrophin mRNA expression in C2C12 myoblast cell after treatment with three lead molecules SG-02, SG-39, and SG-60 at 800 nM concentration for 72 hr compared to piperine at 3 µM and untreated control. (B & C) Dose-dependent utrophin mRNA Upregulation in SG-02 and SG-39 treated C2C12 Cells for 72 hr compared to piperine at 3 µM, and untreated control. In all data sets, significance was calculated using one-way ANOVA, *p< 0.05, **p<0.01, ***p<0.001.

Notably, these lead compounds exhibited a significant elevation in utrophin mRNA expression levels compared to the positive control, piperine, as illustrated in (Figure 2.22 A). To explore the dose-dependent effects, we selected SG-02 and SG-39 due to their similar utrophin mRNA expression profiles. Subsequently, qRT-PCR and Western blot analyses were performed, revealing that both SG-02 and SG-39 induced a dose-dependent upregulation of utrophin mRNA (Figure 2.22 B-C) and protein expression (Figure 2.23 A-D). Specifically, at

the 800 nM concentration, SG-02 exhibited a 2.72-fold increase in utrophin protein expression and a 2.11-fold increase in utrophin mRNA expression. Similarly, SG-39 demonstrated a 2.51-fold increase in utrophin protein expression and a 1.95-fold increase in utrophin mRNA expression. Notably, these lead compounds exhibited a significant elevation in utrophin mRNA and protein expression levels compared to the positive control, piperine.

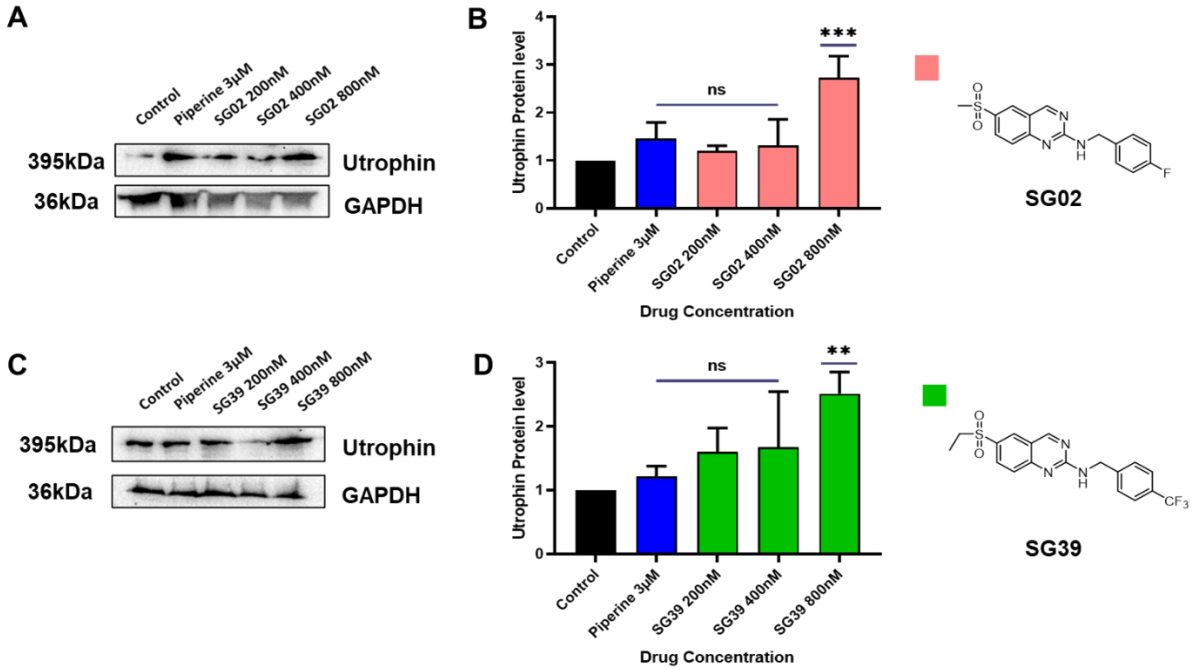


Figure 2.23: Western Blot assay. (a) Western blot analysis comparing protein expression levels of utrophin in C2C12 cells treated with SG-02 in a dose-dependent manner, compared to piperine-treated cells (3 μM), and untreated cells after 72 hr of treatment. (b) Bar diagram representing utrophin expression in terms of fold change for SG-02. (c) Western blot analysis comparing protein expression levels of utrophin in C2C12 cells treated with SG-39 in a dose-dependent manner, compared to piperine-treated cells (3 μM), and untreated cells after 72 hr of treatment. (d) Bar diagram representing utrophin expression in terms of fold change for SG-39; GAPDH was taken as a loading control for all Western blot experiments. In all data sets, significance was calculated using one-way ANOVA, **p<0.01, ***p<0.001.

2.3.8 Utrophin Protein Expression in Human Patient Derived DMD Cell Line

To further evaluate the potential of SG-02 in upregulating utrophin protein, we examined the utrophin expression profile in a human patient-derived DMD cell line (KM1328, cell isolated from paravertebral of 16 year old DMD male patient), which provides more clinically relevant platform for *in-vitro* studies.

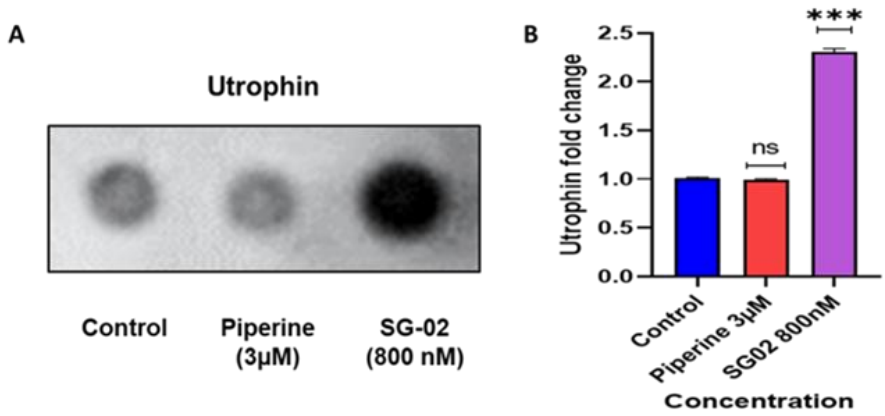


Figure 2.24: Dot blot. Treatment with SG-02 and piperine increases utrophin protein after treating Patient derived human DMD cell line (KM1328) for 72 hr. (a) Relative utrophin expression was assessed by Dot blot analysis for untreated control, piperine (3 μM) and SG-02 (800 nM) treated cells. (b) Bar diagram representing utrophin expression in terms of fold change. In all data sets, significance was calculated using one-way ANOVA, ***p<0.001.

Notably, SG-02 demonstrated the ability to significantly upregulate utrophin protein by up to 2.3 fold at an optimal concentration of 800 nM after 72 hr of treatment compared to untreated controls. In contrast, the positive control, piperine, exhibited an utrophin expression level similar to that of the untreated control (0.99-fold) at a concentration of 3 μM. These results were obtained by isolating proteins from both treated and untreated cells after a 72-hour incubation period and subsequently validating them through dot blot analysis (Figure 2.24 A-B).

2.3.9 Target Validation for Lead Molecule SG-02

Based on the qRT-PCR and Western blot data, we selected SG-02 as our lead molecule over SG-39, as it demonstrated comparatively higher utrophin upregulation profile. Furthermore, during the assessment of the aqueous solubility for all three lead molecules discussed under the ADME segment (2.4.2.12), SG-39 exhibited very poor solubility (> 10 μM), which further strengthened our choice for selection of lead molecule SG-02 for further study of target validation, evaluation of myogenic potential and assessment of other ADME properties (microsomal and serum stability). In order to validate the mechanism of action for our designed hit molecule as an AhR antagonist, we conducted experiments to assess its binding affinity with the AhR: ARNT complex protein. Our findings confirmed that the hit molecule SG-02 indeed shared the same mechanism of action with its sources of inspiration. Here, the binding affinity of our lead molecule was assessed using a fluorescence quenching assay. Through this method, we determined that SG-02 exhibited a binding affinity of 23.988 μM^{-1} and a dissociation constant (K_d) of 41.68 nM calculated for the protein-ligand interaction. These results provide quantitative measurements of the binding strength between our hit molecule SG-02 and the target protein, offering valuable insights into their interaction dynamics (Figure 2.25 B).

Further, to establish the antagonist nature of SG-02 towards AhR protein, we performed co-localization studies with the known AhR agonist ligand ITE (2-(1'H-indole-3'-carbonyl)-thiazole-4-carboxylic acid methyl ester). [34, 19]

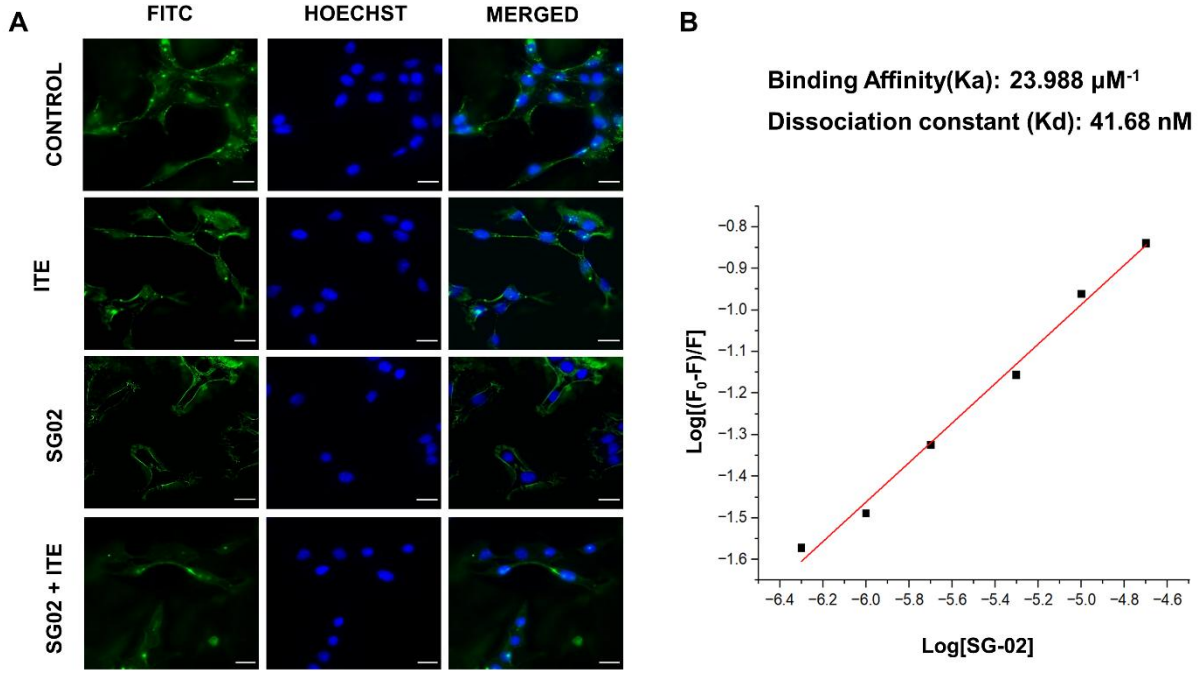


Figure 2.25: SG-02 behaves as an aryl hydrocarbon antagonist. (A) The subcellular localization of AhR induced by SG-02 treatment as examined using immunofluorescence. In C2C12, AhR was predominantly found in the cytoplasm unlike the agonist 2-(1'H-indole-3'-carbonyl)-thiazole-4-carboxylic acid methyl ester (ITE), which promotes nuclear translocation of AhR, SG-02 did not cause an increase in nuclear translocation. Whereas, co-treatment of ITE (1 μM) with SG-02 (800 nM) resulted in the retention of AhR in the cytoplasm. (B) Tryptophan fluorescence quenching assay to determine the binding constant between AhR:ARNT complex and SG-02.

In C2C12 myoblast cells, AhR predominantly localizes in the cytoplasm. Unlike the agonist ITE, which induces nuclear translocation of AhR, antagonist molecule SG-02 did not promote nuclear translocation. Treatment of C2C12 myoblast cells with SG-02 (800 nM) for 2 hr resulted in no AhR localization in the nucleus, while the positive control group treated with the established agonist ITE (1 μM) showed observable nuclear translocation of AhR. Co-treatment of SG-02 (800 nM) with ITE (1 μM) also failed to induce AhR nuclear translocation. This validates the antagonistic property of SG-02 towards AhR (Figure 2.25 A). These experiments collectively established the mechanism of action for the lead molecule, providing insights into its binding affinity and antagonistic properties within the AhR signalling pathway.

2.3.10 Fusion Assay

The fusion of myoblasts into mature myotubes is a critical process involved in muscle development and repair. However, this process is disrupted in dystrophic muscles.[22] The AhR agonist 2,3,7,8-tetrachlorodibenzo-p-dioxin (TCDD) has been demonstrated to inhibit

myotube formation in the C2C12 myoblast cell line by disrupting the fusion process and reducing the expression of myosin heavy chain (MyHC).[35]

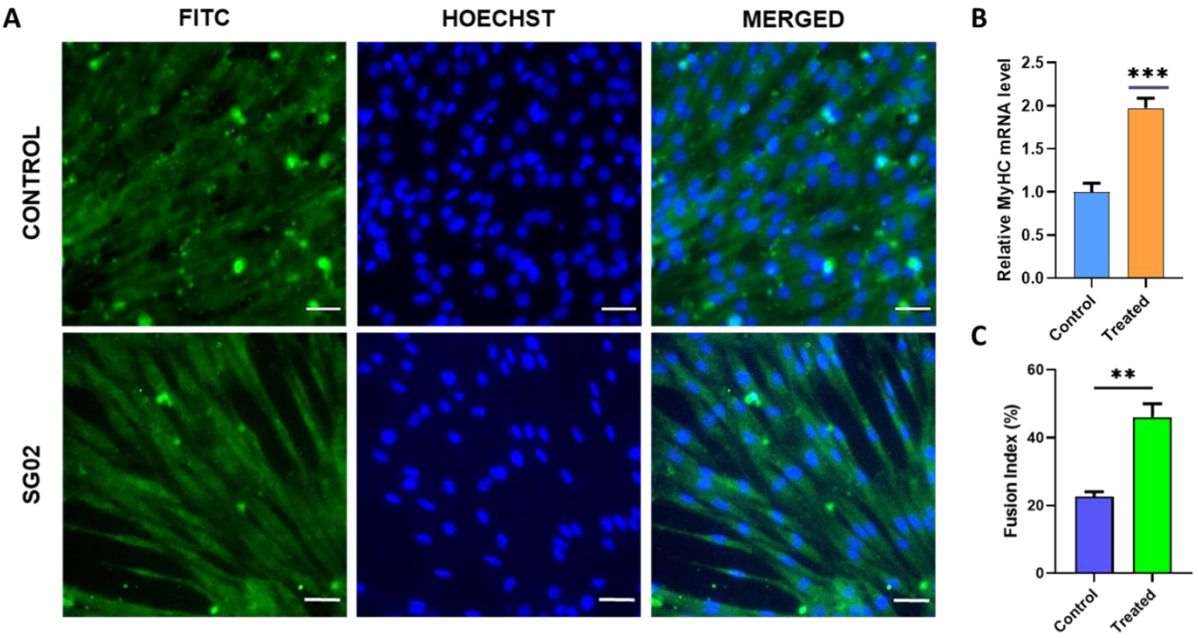


Figure 2.26: Myoblast Fusion. (A) Immunofluorescent image of fused cells, where the cells were labelled with primary antibody to MyHC and secondary Alexa 488 (green) and Hoechst 33258 (blue). Scale bar corresponds to 50µm. Myoblast fusion is observed in the group treated with compound SG-02 (800 nM) for 7 Days. (B) MyHC mRNA expression of SG-02 in C2C12 myoblast cell after treatment with SG-02 in 800 nM concentration for 72 hr shows two fold upregulation in comparison to untreated control. (C) The percent (%) fusion index was determined by calculating the ratio of nuclei detected in the MyHC positive area to the total nuclei count. In all data sets, significance was calculated using t test **p<0.01, and ***p<0.001.

Therefore, assessing the potential of SG-02 as an AhR antagonist holds promise for enhancing the fusion process. Thus, in our study, we investigated the impact of SG-02 on myogenesis and observed an augmentation in the fusion of treated C2C12 myoblast cells into mature myotubes. This improvement in myogenesis was validated through immunocytochemistry analysis and qRT-PCR, specifically examining the expression of myogenic marker, myosin heavy chain (MyHC), at both the protein and mRNA level. Our findings demonstrated that SG-02 enhances myogenesis almost two folds compared to the untreated control after seven days of treatment in differentiation media, suggesting its potential as a therapeutic strategy to address the impaired fusion process in dystrophic muscles apart from upregulating utrophin. (Fig 2.26 A-C). Cell imaging was performed using an Olympus microscope (IX-83) with a 40X objective, and this analysis was carried out using Myocount software, which processed the captured images (Figure 2.27).

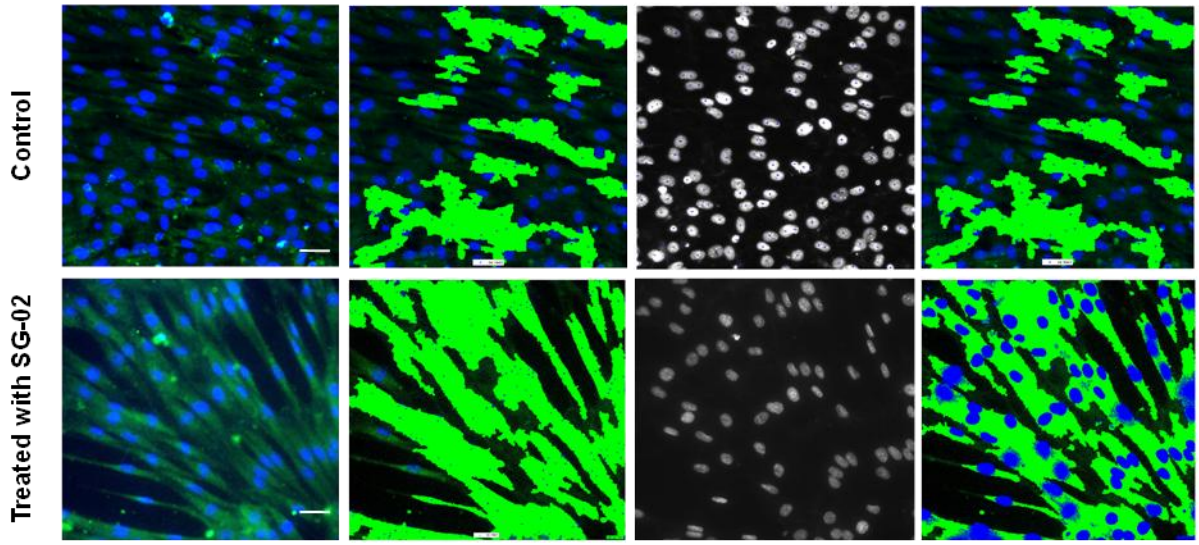


Figure 2.27: Myoblast Fusion Analysis of Lead Molecule SG-02 performed through Myocount software, which processed the captured images based on immunofluorescent image of fused cells. Analysis was calculated in five image per well. Scale bar corresponds to 50µm.

2.3.11 In-Vitro ADME Study

To evaluate the potential of our lead molecule SG-02 as an oral bioavailable drug candidate, we have performed some preliminary in-vitro ADME studies, which include (i) aqueous solubility assay. (ii) microsomal stability assay. (iii) serum stability assay. (iv) lipophilicity assay.

2.3.11.1 Aqueous Solubility Assay

Aqueous solubility of compound plays a significant role in its oral bioavailability and subsequent systemic distribution. Assessment of aqueous solubility is essential for determining the suitability of drug candidate for oral administration. Herein we employ turbidimetric solubility method in determining the aqueous solubility of our three lead molecules SG-02, SG-39 and SG-60. The result from this study revealed that aqueous solubility of our lead molecule SG-02 falls within the range of 30-40 µM, in comparison to the control pyrene thus positioning this molecule in a moderate range of aqueous solubility. Whereas SG-39 exhibited least aqueous solubility <10 µM, and SG-60 displayed aqueous solubility up to 50 µM. (Figure 2.28 A)

2.3.11.2 Microsomal Stability Assay

During microsomal incubations, we monitored the rate at which a test compound was cleared over a specific period of time. The resulting data was then utilized to calculate the intrinsic clearance of the compound. This parameter is essential for understanding the compound's pharmacokinetic profile and potential for oral bioavailability. By determining the intrinsic clearance, we gained insights into the compound's clearance rate and its potential for further

development as a viable drug candidate. To evaluate the microsomal stability of our lead molecule, SG-02, we conducted an incubation study using microsomes derived from rat liver. The reaction was initiated by the addition of NADPH and monitored over a period of 60 min at 37 °C. Our observations revealed that SG-02 exhibited requisite stability during microsomal incubation. Further analysis of the data revealed that the half-life of SG-02 during microsomal incubation was determined to be 210 min. Additionally, the calculated hepatic intrinsic clearance (h CL_{int}) of SG-02 was found to be 6.66 µL/min/mg. This finding suggests that SG-02 holds promise as an oral bioavailable drug candidate, as it demonstrates favourable stability in microsomal environments. These results provide valuable insights into the compound's metabolic behaviour and supports its potential for further development as an orally administered medication (Figure 2.28 B).

2.3.11.3 Serum Stability Assay

In addition to undergoing metabolism in the liver, compounds can also undergo degradation and modification by enzymes present in the plasma. These enzymatic processes in the plasma contribute to the overall clearance and elimination of compounds from the systemic circulation. Understanding the involvement of plasma enzymes in the metabolism of compounds is crucial for assessing their stability and potential for therapeutic efficacy. We performed a human plasma stability assay to assess the stability of our lead molecule, SG-02. Incubation of SG-02 with human serum over various time intervals revealed that the compound remained stable up to seventy percent after 2 hr of incubation. This study emphasizes the compound's resilience within the plasma environment (Figure 2.28 C).

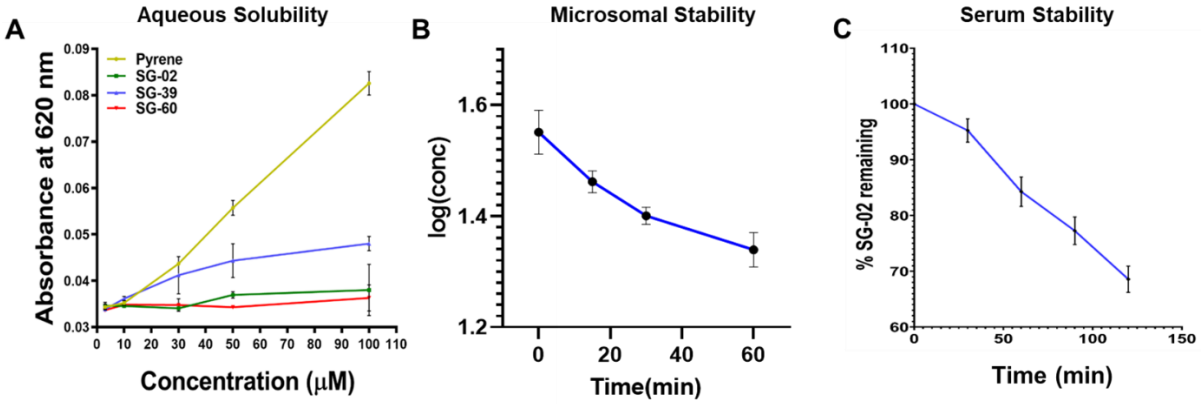


Figure 2.28: Biophysical characterization of lead molecule SG-02. (A) Turbidity assay to determine aqueous solubility of three lead molecules SG-02, SG-39, and SG-60 with pyrene as control. After 2 hours of incubation in PBS, absorbance was measured at 620 nm. (B) Microsomal stability of lead molecule analyzed by microsomal incubation of SG-02 over a period of 60 min. (C) Serum stability of SG-02 displays that SG-02 is intact upto 70% after two hours of incubation.

2.3.11.4 Lipophilicity Assay

The assessment of lipophilicity plays a crucial role in understanding the molecular properties of compounds. By measuring Log D, we gained insights into the lipophilic nature of a compound and its propensity for partitioning between different environments. An ideal lipophilicity range often falls within Log D values of 0 to 3.[36] In our study, SG-02 demonstrated distribution coefficient values of log D @ $pH_{7.4}$ = 0.2 in the cyclohexane/PBS system and log D @ $pH_{7.4}$ = 2.46 in the octanol/PBS system. This log D value of lead molecule SG-02 renders it as fit drug candidate for oral absorption and cell membrane permeation (Table 1.4).

Compound	Aqueous solubility (µM)	Microsomal Stability, h Cl_{int} (µl/min/mg)	Microsomal Stability, h $T_{1/2}$ (min)	Plasma Stability [a]	log D @pH 7.4[b]	log D @pH 7.4[c]
SG02	30-40 µM	6.66	210	69.18	0.2 ± 0.03	2.46±0.05

Table 2.4: Preliminary ADME properties such as Solubility, microsomal stability, plasma stability for lead molecule SG-02. [a] Mean % remaining at 2 h in human plasma, [b] Cyclohexane/PBS, [c] Octanol/PBS.

2.4 Experimental Section

2.4.1. Materials

Chemistry

All starting materials, reagents, and solvents were purchased from commercial suppliers and used without further purification. The compounds underwent routine analysis through thin-layer chromatography (TLC) performed on precoated TLC plates (Merck Silica Gel 60 F254, layer 0.20 mm) and then visualized under a UV lamp (λ = 254 and 365 nm). Solutions obtained after reactions and extractions were concentrated using a rotary evaporator. Organic solutions were dried using anhydrous sodium sulfate. ^{1}HNMR and ^{13}CNMR spectra were acquired using a Bruker Advance 500 MHz spectrometer at a temperature of 300 K, with TMS serving as the internal standard. Mass spectra were recorded utilizing an Agilent Technologies electrospray ionization ESI; Q-TOF mass spectrometer instrument (G6530C). For high-performance liquid chromatography (HPLC) analysis, a Shimadzu C18 column (150 mm × 4.6 mm × 5 µm) was employed. The mobile phase consisted of a gradient of 40-70% acetonitrile in an aqueous solution, and the detection wavelength was set at 254 nm. The flow rate was maintained at 1 mL/min, and the temperature of the column was set at 30 °C. The pressure applied ranged from 85 to 142 kgf. The purity of all compounds was found to be greater than 95%, as determined by HPLC analysis.

Biology

3-(4,5-dimethylthiazol-2-yl)-2,5-diphenyl tetrazolium bromide (MTT) (M2128, Sigma), Collagen type I (TC343, Himedia), Janus Green B (201677, Sigma), Triton X-100 (BB031, Himedia), Bovin Serum Albumin (BSA) (83803, SRL), Antimycotic antibiotic solution (Himedia A002), Fetal Bovine Serum (Invitrogen 2023-01-30), Penicillin Streptomycin solution (Invitrogen 15140-122), Trypsin EDTA Solution (Sigma T4174), Formaldehyde solution (Sigma-Aldrich 47608), Tween 20 detergent (Sigma Aldrich P9416), Glycine (Himedia MB013), Tris Base (Himedia MB029), 2-Mercaptoethanol (MB041, Himedia), Protease/Phosphatase Inhibitor Cocktail (100X) (5872SA, CST), Ammonium Persulfate (SRL 7727-54-0), TEMED (Sigma Aldrich T7024), Acrylamide/Bis-acrylamide solution [SRL 67394 (0124437)], Sodium Dodecyl Sulfate (Sigma Aldrich L3771), Bromophenol Blue (Sigma Aldrich 114391), Immobilon Western HRP Substrate (Millipore WBLU F0500), PVDF Membrane (Millipore). Utrophin Antibody (SC-33700, Santa Cruz), AhR Antibody (SC-133088, Santa Cruz,), Myosin Heavy Chain Antibody (SC-376157, Santa Cruz), HRP conjugated secondary Antibody (Anti-Mouse IgG HRP linked, CST 7076), Anti-Rabbit IgG HRP linked, (CST-7074), Goat anti-mouse IgG H&L Alexa Fluor® 488, (Thermo, A11029), Hoecsht 33258 (ab228550, Abcam).

2.4.2 Methods

2.4.2.1 Synthesis of molecular library

General Procedure for the synthesis of 6-bromoquinazolin-2-amine (b), Scheme-1, Step 1:

5-bromo-2-fluorobenzaldehyde **(a)** (1gm, 4.92 mmol, 1 eq) was dissolved in DMA (20 mL), followed by addition of guanidine carbonate (7.6 gm, 7.38 mmol, 1.5 eq), then the reaction mixture was heated at 150 ^{0}C for 5 h. The reaction progress was monitored by TLC, after completion. The reaction mixture was cooled and quenched with ice cold water and allowed to stir for 30 min. The yellow precipitate thus obtained was filtered off and dried to get the title compound (0.8 gm, 72% yield). [28]

General Procedure for the synthesis of 6-bromo-2-chloroquinazoline (c), Scheme-1, Step 2:

6-bromoquinazolin-2-amine (0.75gm, 3.36 mmol, 1 eq) was dissolved in DCM-DMF (8:2), followed by addition of n-Bu4NCl (1.12gm, 4.03 mmol, 1.2eq), TMSCl (1.7 mL, 13.44 mmol, 4 eq), followed by dropwise addition of t-BuONO (1.18 mL, 10.08 mmol, 3eq). Stir the reaction mixture for 15 min and then heat at 50 °C for 1-1.5 hr until consumption of starting material (TLC). After consumption, the reaction mixture was cooled and added saturated $NaHCO_3$, and the latter was extracted with DCM (2×100 mL). The combined organic layers were dried with anhydrous sodium sulfate and concentrated under reduced pressure. The crude obtained was purified by column chromatography (40% ethylacetate-hexane) to get the desired compound (0.37gm, 45% yield).[29]

General Procedure for synthesis of N-benzyl/aryl-6-bromoquinazolin-2-amine derivatives (d), Scheme-1, step 3:

6-bromo-2-chloroquinazoline (0.37gm, 1.51 mmol, 1 eq) was dissolved in ethanol, followed by the addition of differently substituted benzyl/aryl (3 eq) amines and allowed to heat at 150 ^{0}C, for 24-48 hr, until the consumption of starting material (TLC). After consumption of starting material, the reaction mass was evaporated under reduced pressure to remove ethanol. And, later the reaction mixture was washed with 1(N) NaOH to remove any unreacted amine, followed by extraction with 3×25 mL EtOAc. The organic layers were dried over anhydrous sodium sulfate and evaporated under reduce pressure to get the desired compounds (0.35-0.45gm, 75-88% yield).[30]

General Procedure for the synthesis of the desired N-benzyl/aryl substituted-6-(methyl/ethylsulfonyl)quinazolin-2-amines (e), Scheme-1, Step 4:

The pure N-benzyl/aryl-6-bromoquinazolin-2-amine derivative (0.2gm, 1 eq) obtained in the previous step was dissolved in dry DMF, followed by the addition of L-Proline (2 eq), Potassium carbonate (4 eq), sodium ethane/methane sufinate (2 eq) and allowed to degas under nitrogen atmosphere for 10 min. Then CuI (1eq) was added to the reaction mixture and again degas for 10 min, and heated in pressure tube at 80-90 ^{0}C for 12 hr. After the completion of starting material, the reaction mass was filtered off over celite bed and the filtrate was kept with cold water. Later the reaction mass was extracted by (3×30 mL) with ethyl acetate, and organic layers were dried over anhydrous sodium sulfate and evaporated over reduced pressure. The crude was purified by column chromatography to get the desired final compounds (0.1 -0.12 gm, 50-60% yield) at 40-50% EtOAc/hexane.[31]

General Procedure for the synthesis of N-(4-bromophenyl)cinnamamide (g), Scheme-2, Step 1:

A solution of cinnamoyl chloride (0.532gm, 3.197 mmol, 1.1 eq) in DCM (5 mL) was added drop wise to a stirring mixture of pyridine (0.25 mL, 3.197 mmol, 1.1 eq) and DMAP (0.325 mg, 0.29 mmol, 0.1 eq) in DCM (5 mL) at 0˚C under inert atmosphere. The reaction mixture was then allowed to stir for 15 min, followed by dropwise addition of 4-bromo-aniline **(f)** (0.5gm, 2.906 mmol, 1eq) in DCM (5 mL). After allowing the reaction mixture to stir at 0˚C for another 15 min, it was allowed to warm to room temperature and stirred for another 2 hr. After the completion of the starting material as monitored by TLC, the reaction mass was diluted with DCM, and the organic layer was washed with 1(N) NaOH, followed by 1 (N) HCl. The organic layer was then washed with brine, and the extracted organic layer was dried over anhydrous sodium sulfate, and evaporated under reduced pressure to afford the title compound (0.85 gm, 96 % yield) and was proceeded for the next step without further purification.[32]

General Procedure the synthesis of 6-bromoquinolin-2(1H)-one (h), Scheme-2, Step 2:

The amide (0.77 gm, 2.54 mmol, 1 eq) from the previous step was dissolved in solvent chlorobenzene (15 mL) followed by the addition of alumunium chloride (2.06 gm, 15.45 mmol, 6.1 eq) under an inert atmosphere. Then, the reaction mixture was refluxed, and the colour of the reaction mixture was observed to quickly turn to yellow then black. After completion of the starting material in 2 hr, monitored by TLC, the reaction mass was allowed to cool down.

Then, the reaction mixture was concentrated under reduced pressure at rotary evaporator up to 5 mL, then poured into ice. The resulting aqueous suspension was filtered. The solid was dried under vacuum to afford the product as a light orange solid (0.35 gm, 61% yield).[33]

General Procedure for the synthesis of 6-bromo-2-chloroquinoline (i), Scheme-2, Step 3:

The intermediate lactam 6-bromoquinolin-2(1H)-one (0.325 gm, 1.450 mmole, 1 eq) obtained from the previous step was placed in round bottom flask, and slowly phosphoryl chloride (12 mL, 14.5 mmol, 10 eq) was added and allowed to stir. Then, the reaction mixture was allowed to heat under reflux condition for 1.5- 2 hour. Then, the reaction mixture was allowed to cool down to RT and quenched by a very slow addition of ice to the reaction mixture. The precipitate obtained was filtered off, and dried under vacuum to afford the title compound (0.33 gm, 94% yield).[33]

General Procedure for the synthesis of N-substituted-6-bromoquinolin-2-amine derivatives (j), Scheme-2, Step 4:

6-bromo-2-chloroquinoline (0.33gm, 1.37 mmol, 1eq) was dissolved in ethanol, followed by the addition of differently substituted benzyl/aryl (3 eq) amines and allowed to heat at 150 ^{0}C, for 24-48 hr, until the consumption of starting material (TLC). After consumption of starting material, the reaction mass was evaporated under reduced pressure to remove ethanol. And, later the reaction mixture was washed with 1(N) NaOH to remove any unreacted amine, followed by extraction with 3×25 mL EtOAc. The organic layers were dried over anhydrous sodium sulfate and evaporated under reduce pressure to get the desired compounds (0.35-0.45gm, 75-88% yield).[30]

General Procedure for the synthesis of N- substituted-6-(methyl/ethylsulfonyl)quinolin-2-amine derivatives (k), Scheme-2, Step 5:

N-substituted-6-bromoquinolin-2-amine derivatives (1eq) obtained in the previous step was dissolved in dry DMF, followed by the addition of L-Proline (2 eq), Potassium carbonate (4 eq), sodium ethane/methane sufinate (2 eq) and allowed to degas under nitrogen atmosphere for 10 min. Then CuI (1eq) was added to the reaction mixture and again degas for 10 min, and heated in pressure tube at 80-90 ^{0}C for 12 hr. After the completion of starting material, the reaction mass was filtered off over celite bed and the filtrate was kept with cold water. Later the reaction mass was extracted by (3×30 mL) with ethyl acetate, and organic layers were dried over anhydrous sodium sulfate and evaporated over reduced pressure. The crude was purified by column chromatography to get the desired final compounds (0.1 -0.12 gm, 50-60% yield) at 40-50% EtOAc/hexane.[31]

2.4.2.2 Cell Viability

Cytotoxicity assessment of quinazoline and quinoline-based small molecules was conducted using the MTT reduction method with C2C12 myoblast cells. The MTT (3-[4,5-dimethylthiazol-2-yl]-2,5 diphenyl tetrazolium bromide) dye is reduced by the NAD(P)H-dependent oxidoreductase enzyme present in live cells, resulting in the formation of purple-colored formazan crystals from the initial yellow color of the dye. This reduction process does not occur in dead cells due to the absence of the NAD(P)H-dependent oxidoreductase enzyme. For the experimental setup, C2C12 myoblast cells were plated in a 96-well plate at a

density of 5×10^3 cells per well and incubated for 24 hr under conditions of 37 °C and 5% CO2. Following the 24-hour plating period, the cells were treated with varying concentrations (0.78, 1.56, 3.125, 6.25, 12.5, 25, 50, 100 µM) of each small molecule and further incubated for 24 hr. To assess cytotoxicity, 50 µL of MTT solution (5 mg/mL) prepared in PBS was added to each well and incubated for an additional 4 hr at 37 °C. Subsequently, the MTT solution was removed, and 100 µL of DMSO/Methanol (1:1 v/v) was added to each well to dissolve the formazan crystals.[37] The absorbance was measured at 570 nm wavelength using a microplate reader (Thermo Scientific; Varioskan LUX).

Cell viability (%) = {[A570 (treated cells) – A570 (blank)]/ [A570 (control cells) – A570 (blank)] × 100.

2.4.2.3 Screening of Molecular Library by High-throughput In-Cell ELISA Technique

The In-Cell ELISA assay was conducted for screening a library of small molecules with modifications based on a previously reported protocol.[38] In this procedure, C2C12 myoblast cells were seeded in a white flat-bottomed 96-well plate at a density of 5×10^3 cells per well and incubated for 24 hr at 37°C with 5% CO_2. Following the 24-hour plating period, the cells were treated with each small molecule at a concentration of 800 nM for 72 hr. The cells were subsequently fixed with 4% paraformaldehyde for 15 min, washed twice with 1xPBS, and permeabilized with 1X permeabilization buffer for 30 min at 300 rpm on a shaker. After permeabilization, blocking was performed using a 2% BSA blocking buffer for 2 hr at room temperature. The cells were then washed once with 1X wash buffer and incubated overnight at 4°C with a primary antibody against utrophin. Following the primary antibody incubation, the cells were washed three times with 1X wash buffer and then incubated with an HRP-conjugated secondary antibody for 1 hour at room temperature. After the secondary antibody incubation, the cells were washed three times with wash buffer and then OPD solution is added, followed by a 15-min incubation at 37 °C. The reaction was halted using 8% H_2SO_4. The absorbance at 492 nm was measured using a microplate reader (Thermo SCIENTIFIC; VARIOSKAN LUX). The cell number was normalized using Janus Green B by measuring the absorbance at 595 nm.

2.4.2.4 RNA Extraction and Reverse Transcription-Polymerase Chain Reaction

Total RNA was isolated from treated C2C12 myoblast cells using the Invitrogen PureLink RNA Mini Kit following the manufacturer's instructions. The concentration and purity of the RNA were determined by measuring the A260/A280 ratio using a Nanodrop spectrophotometer. Subsequently, 300 ng of the total RNA was utilized to synthesize cDNA employing the RevertAid First Strand cDNA Synthesis Kit, following the manufacturer's protocols. For quantitative polymerase chain reaction (qPCR), a BioRad CFX96 Real Time System was employed, utilizing the BioRad iTaqTM Universal SYBR Green Supermix for the amplification reaction.[39] Utrophin amplification and the normalization against the housekeeping gene GAPDH were conducted in triplicate (n = 3). The following primer pairs were employed: for Utrophin (Mouse), forward 5′ AGAGCACTATGACCCCTCCC 3′ and

reverse 5′ CATCTGGGCCAGTCGTGTAG 3′, and for GAPDH (Mouse), forward 5′ CTTCGGGCCACGCTAATCTC 3′ and reverse 5′ CCAATACGGCCAAATCCGTTC 3′. The obtained values were processed according to the $2^{-\Delta\Delta CT}$ method.[40] Statistical analysis was performed using One-Way ANOVA and P values were calculated using Prism 8.0 software.

2.4.2.5 Protein Isolation and Western Blot Analysis

To assess the impact of small molecules on utrophin protein expression, Western blot analysis was performed. Cellular proteins were extracted from treated C2C12 myoblast cells through lysis using RIPA buffer supplemented with 1% protease phosphatase inhibitor cocktail. The quantification of the extracted proteins was carried out using the Bradford assay. For utrophin analysis, a total of 40 µg of protein extract was resolved on an 8% SDS-PAGE gel, while for GAPDH analysis, 12-15% SDS-PAGE gels were employed. The resolved proteins were subsequently transferred onto PVDF (Polyvinylidene difluoride) membranes. Blocking was performed using 5% BSA in TBS-T buffer solution for a duration of 2 hr at room temperature. Following blocking, the PVDF membrane was probed with primary antibodies targeting utrophin (diluted 1:1000) and GAPDH (diluted 1:5000) at 4 °C overnight. After undergoing three washes with 1X TBS-T, the membrane was subjected to incubation with an HRP-conjugated anti-mouse secondary antibody (diluted 1:5000) for 2 hr at room temperature. Subsequently, the membrane was washed with 1X TBS-T buffer, and protein detection was executed through chemiluminescence using immobilon Forte Western HRP substrate in a BioRad ChemiDoc system.[39] Densitometric analysis of the acquired images was performed using ImageJ software, with GAPDH utilized as the loading control.

2.4.2.6 Fluorescence Quenching Assay of SG-02 with AhR: ARNT

The interaction between the SG-02 molecule and recombinant AhR: ARNT protein was assessed utilizing a fluorescence microplate reader with excitation at 280 nm and emission at 310 nm. A concentration of 1 µM protein was subjected to incubation with varying concentrations of the molecule (20, 10, 5, 2, 1, 0.5 µM) for a duration of 30 min. This incubation was carried out in a black 96-well plate containing a buffer consisting of 20 mM Tris pH 8, 200 mM NaCl, and 1% DMSO. Subsequent to the incubation, fluorescence emission was measured, and the dissociation constant (K_d) values were computed using a modified Stern–Volmer equation. The obtained data were further analyzed utilizing OriginPro 8.5 software.[19]

2.4.2.7 Immunofluorescence Analysis of AhR Localization

C2C12 myoblast cells were cultured on confocal discs at a seeding density of 1×10^3 cells and then incubated for 24 hr at 37 °C under 5% CO_2 conditions. After 24 hr of plating, the cells were treated with SG-02 (800nM), ITE (1µM), and a combination of both compounds (with a final DMSO concentration of 0.02%) in media and control. After a 2-hour exposure, the cells

were fixed with 4% paraformaldehyde for 15 min at 37 °C, washed twice with 1x PBS, and subsequently permeabilized with 0.1% Triton X-100 containing 1% BSA in PBS for 15 min. The cells were again washed with 1x PBS and then incubated with a primary antibody targeting AhR (1:500) overnight at 4 °C. Following the primary antibody incubation, the cells were washed with 1x PBS and subsequently incubated with an Alexa Fluor 488 conjugated anti-mouse secondary antibody. Nuclear staining was performed using Hoechst 33258 for 30 min. After a final wash with 1x PBS, fluorescence images were captured using a fluorescence microscope (Olympus IX83) with a magnification of 60X.[19]

2.4.2.8 Myoblast Fusion

C2C12 myoblast cells were seeded at a density of 3×10^3 cells onto 18 mm cover slips coated with 1% collagen. Once the cells reached 80-90% confluency, they were treated with SG-02 (800 nM) in differentiation media for a duration of 7 days.[41] Following the treatment period, the cells were fixed with 4% paraformaldehyde for 15 min at 37 °C, washed twice with 1X PBS, and subsequently permeabilized with a solution containing 0.1% Triton X-100 and 1% BSA in PBS for 15 min. After another round of washing with 1X PBS, the cells were incubated with a primary antibody targeting MyHC (1:500) overnight at 4 °C. Following the primary antibody incubation, the cells were washed with 1X PBS and then exposed to an Alexa Fluor 488 conjugated anti-mouse secondary antibody. Nuclear staining was conducted using Hoechst 33258 for a period of 30 min. After a final wash with 1X PBS, fluorescence images were acquired using a fluorescence microscope (Olympus IX83) at a magnification of 40X.

2.4.2.9 MyHC RNA Extraction and Reverse Transcription-Polymerase Chain Reaction

Total RNA was extracted from the treated C2C12 myoblast cells after treatment with SG-02 at 800 nM concentration for 72 hours using the PureLink RNA Mini Kit (Cat. No. 12183018A, Invitrogen) according to the manufacturer's instructions. The concentration and the purity of the RNA (A260/A280 > 1.8) were determined by a NanoDrop 1000 spectrophotometer (Thermo Fisher Scientific). Using 300 ng of total RNA, cDNA was synthesized using the iScript cDNA Synthesis Kit (Cat. No. #1708890, Bio-Rad) according to the manufacturer's instructions. Diluted the cDNA 10-fold with nuclease-free water for RT-qPCR analysis. A reaction mix of 10 µL was prepared for the assay using 5 µL of iTaq™ Universal SYBR Green Supermix (2x), 0.5 µL of each specific primer of a concentration of 10 µM, and 4 µL of the diluted cDNA. The PCR was conducted using a standard fast protocol. This includes 95 °C for 20 s for initial heating followed by 40 cycles of amplification that comprised of the following: 95 °C for 3 s and annealing temperature of 60 °C for 30s followed by 70 °C for 5s. The expression levels were calculated against GAPDH and used as an endogenous control. Relative levels of mRNA expression were estimated by the $2^{-\Delta\Delta Ct}$ method.

Gene	Forward 5′-3′	Reverse 5′-3′	Accession No.
MYH3	GCTTGTGGGCGGAGGTCT	AGCAGCTATGCCGAACACTT	NM_002470.4

2.4.2.10 Protein Isolation from Patient Derived Human Cell Line (KM1328) and Dot blot Analysis

Immortalized human myoblast DMD cell line (KM1328) were provided by V. Mouly at the Institut de Myologie in France. 3×10^5 cells were seeded in per well of 6 well plate and was cultured in skeletal muscle cell growth media (c-23060, Promocell) for 24 hr. Subsequently, the cells were treated with SG-02 at a concentration of 800 nM and piperine at 3 µM, following the 24-hour treatment interval, and then incubated for 72 hr. After the treatment period, the protein was isolated using RIPA buffer supplemented with protease and phosphatase inhibitors, and its concentration was quantified using the Bradford assay. For the dot blot analysis, 2 µL of the eluted sample was spotted onto a nitrocellulose membrane. The membrane was blocked with 5% BSA and then incubated with the anti-AhR primary antibody overnight. The blots were visualized by incubating them with an HRP-conjugated secondary antibody for 2 hr and imaged using the G-Box Chemi XRQ system (Syngene, UK). Densitometric analysis of the acquired images was performed using ImageJ software.

2.4.2.11 Microsomal Stability Assay

To check the *in vitro* drug metabolism, microsomal stability assay was performed of lead molecule SG-02. Over microsomal incubations, the rate of clearance of a test compound over time was observed, and these data were used to calculate intrinsic clearance. Test compound 5µM in PBS was pre-incubated with 20 mg/mL microsome in the water bath at 37°C for 5 min. The reaction was then initiated by adding 20mM NADPH, followed by further incubation at 37°C with gentle agitation for 60 min. The reaction was terminated at regular intervals of 0, 15, 45 and 60 min by the addition of 200 µL of ethylacetate. The resulting samples were then centrifuged at 3000 rpm for 5 min, and the supernatant was collected for analysis using LC-MS and HPLC. The disappearance pattern of the test compound was tracked over the 60-min duration. [42]

2.4.2.12 Aqueous Solubility Assay

The aqueous solubility of the lead molecules was determined using a turbidity assay. A stock solution of the compounds at a concentration of 10 mM was prepared in DMSO. Subsequently, appropriate dilutions of the DMSO stock solution were made in 0.01 M PBS buffer to achieve concentrations of 3, 10, 30, 50, and 100 µM. These solutions were then incubated at 37 °C for 2 hr. After the incubation period, the absorbance of each dilution was measured at 620 nm to generate a solubility profile. As a reference dataset, pyrene, known for its low aqueous solubility, was used.[43]

2.4.2.13 Serum Stability Assay

Apart from undergoing hepatic metabolism, compounds can also undergo degradation and modification by enzymes present in plasma. So, to check the human plasma stability of lead molecule SG-02, a serum stability assay was conducted. For that, a stock solution of 10 mM in DMSO was prepared. From that stock solution, a test compound stock (50 µM) was prepared by diluting it in acetonitrile. The frozen plasma was thawed at room temperature, followed by centrifugation at 14000 rpm at 4 °C for 15 min. Next the clear supernatant fraction roughly 90 % was transferred to a separate tube and utilized for the assay. Pre incubate the plasma at 37 ^{0}C for 15 min, then add the test compound and withdraw sample 100 µL each from the incubated mixture kept at 37°C at 0 min, 60 min, and 120 min and precipitated immediately with ice cold 100 µL acetonitrile. This precipitated mixture was vortexed for 1 min and then centrifuged at 12000 rpm for 10 min. The supernatant was recovered and stored at -20 °C for further analysis by LC-MS and HPLC. The amount of intact test compound SG-02 was monitored over 120 min.[44]

2.4.2.14 Lipophilicity assay

Equal volumes of sodium phosphate buffer (pH 7.4) and n-octanol were mixed thoroughly by vortexing in a micro centrifuge tube. The mixture was thoroughly homogenized and subsequently subjected to a phase separation process, where it was allowed to pre-saturate over a period of 24 hr. The resultant phases were subsequently transferred into two separate containers. A stock solution of the test substance (10 mM) was prepared using 100% DMSO and stored at 4 °C. For the experimental procedure, 500 µL of the organic phase (1-octanol) was added to a 2 mL micro centrifuge tube. Subsequently, 500 µL of buffer and 15 µL of the test substance were added. The tube was then subjected to vortexing for 1 hour at a speed of 1200 rpm using a plate shaker. After the incubation period, the samples were subsequently subjected to a 20-min equilibration period. After the process of equilibration, centrifugation was conducted at a speed of 4000 rpm for a duration of 30 min in order to achieve a thorough separation of the phases. Subsequently, the samples were subjected to analysis employing LC-MS and HPLC techniques. The same procedural steps were executed during the determination of the Log D value for the Cyclohexane/PBS system.[45]

2.4.2.15 Molecular Docking Studies

Molecular Docking Analysis with Aryl hydrocarbon receptor mediated gene activation protein (PDB ID: 5NJ8) and the designed lead molecule is done after modifying the 5NJ8 PDB by removing the bound DNA from its crystal structure using Autodock Vina 1.1.2.36. A grid box volume of 83 × 88 × 80 was set around the receptor protein structure (PDB ID: 5NJ8). All the docking images were observed and processed in PyMOL.

2.5 Conclusion

Upregulation of the utrophin protein, a paralogue protein of dystrophin, has emerged as a potential therapeutic approach for DMD, holding the potential to treat the universal DMD population irrespective of various mutation types. The limitations encountered with the first-generation drug, ezutromid, inspired us to develop novel utrophin modulators outside the ezutromid family. Drawing inspiration from AhR antagonist ligands and other utrophin-upregulating drug molecules, we designed, synthesized, and evaluated small molecules based on the quinazoline and quinoline cores. Hit molecules were identified from the library of synthesized molecules utilizing a high-throughput screening method based on the In-cell ELISA technique in the C2C12 myoblast cell line. Through RT-PCR and Western blot analysis, the lead compound SG-02 identified was confirmed to upregulate utrophin mRNA by 2.11-fold and protein by up to 2.7-fold at 800 nM in a dose dependent manner. Remarkably, this represents the highest fold change observed at lower doses within the nanomolar range. The efficacy of the hit molecule SG-02 was further evaluated in a human patient-derived DMD cell line (KM1328), where it demonstrated the ability to upregulate utrophin protein up to 2.3-fold at a same optimum concentration of 800 nM compared to the untreated control. Validation of the target for the lead molecule was achieved by measuring its binding affinity with the AhR protein and confirming its antagonistic role through co-localization studies with the known AhR agonist ligand, ITE. Furthermore, SG-02 also demonstrated notable potential in promoting myogenesis, a critical process for muscle growth and repair. This dual efficacy of SG-02 advocates its potential in both utrophin upregulation and myogenesis. Preliminary ADME assessment conducted supports SG-02 as a promising oral bioavailable drug candidate.

Altogether, our study presents the design, synthesis, and *in vitro* evaluation of novel quinazoline and quinoline core-based compounds with the ability to upregulate utrophin protein. The lead molecule, SG-02, exhibited significant utrophin upregulation, myogenic potential, and holds oral bioavailability attribute, signifying its candidacy as a potential therapeutic agent for DMD.

2.6 References

1. Duan, D.; Goemans, N.; Takeda, S.I.; Mercuri, E; Aartsma-Rus, A., Duchenne muscular dystrophy. *Nat. Rev. Dis. Primers*. **2021,** *7*(1), 13.

2. Flanigan, K.M.; Dunn, D.M.; Von Niederhausern, A.; Soltanzadeh, P.; Gappmaier, E.; Howard, M.T.; Sampson, J.B.; Mendell, J.R.; Wall, C.; King, W.M; Pestronk, A., Mutational spectrum of DMD mutations in dystrophinopathy patients: application of modern diagnostic techniques to a large cohort. *Hum. Mutat*. **2009,** *30* (12), 1657-1666.

3. Nowak, K. J.; Davies, K. E., Duchenne muscular dystrophy and dystrophin: pathogenesis and opportunities for treatment. *EMBO Rep.* **2004,** *5* (9), 872-6.

4. Bushby, K.; Finkel, R.; Birnkrant, D. J.; Case, L. E.; Clemens, P. R.; Cripe, L.; Kaul, A.; Kinnett, K.; McDonald, C.; Pandya, S.; Poysky, J.; Shapiro, F.; Tomezsko, J.; Constantin, C., Diagnosis and management of Duchenne muscular dystrophy, part 1: diagnosis, and pharmacological and psychosocial management. *Lancet. Neurol.* **2010,** *9* (1), 77-93.

5. Cossu, G.; Sampaolesi, M., New therapies for Duchenne muscular dystrophy: challenges, prospects and clinical trials. *Trend. Mol. Med.* **2007,** *13* (12), 520-526.
6. Monaco, A. P.; Neve, R. L.; Colletti-Feener, C.; Bertelson, C. J.; Kurnit, D. M.; Kunkel, L. M., Isolation of candidate cDNAs for portions of the Duchenne muscular dystrophy gene. *Nature* **1986,** *323* (6089), 646-50.
7. Mah, J. K., Current and emerging treatment strategies for Duchenne muscular dystrophy. *Neuropsychiatr. Dis. Treat.* **2016,** *12*, 1795-807.
8. Guiraud, S.; Davies, K. E., Pharmacological advances for treatment in Duchenne muscular dystrophy. *Curr. Opin. Pharmacol.* **2017,** *34*, 36-48.
9. Min, Y. L.; Bassel-Duby, R.; Olson, E. N., CRISPR Correction of Duchenne Muscular Dystrophy. *Annu. Rev. Med.* **2019,** *70*, 239-255.
10. Guiraud, S.; Roblin, D.; Kay, D. E., The potential of utrophin modulators for the treatment of Duchenne muscular dystrophy. *Expert. Opin. Orphan Drugs.* **2018,** *6* (3), 179-192.
11. Ryder, S.; Leadley, R. M.; Armstrong, N.; Westwood, M.; de Kock, S.; Butt, T.; Jain, M.; Kleijnen, J., The burden, epidemiology, costs and treatment for Duchenne muscular dystrophy: an evidence review. *Orphanet J. Rare Dis.* **2017,** *12* (1), 79.
12. Blake, D. J.; Tinsley, J. M.; Davies, K. E., Utrophin: a structural and functional comparison to dystrophin. *Brain Pathol.* **1996,** *6* (1), 37-47.
13. Tinsley, J.; Deconinck, N.; Fisher, R.; Kahn, D.; Phelps, S.; Gillis, J. M.; Davies, K., Expression of full-length utrophin prevents muscular dystrophy in mdx mice. *Nat. Med.* **1998,** *4* (12), 1441-4.
14. Leung, D. G.; Wagner, K. R., Therapeutic advances in muscular dystrophy. *Ann. Neurol.* **2013,** *74* (3), 404-11.
15. Deconinck, N.; Tinsley, J.; De Backer, F.; Fisher, R.; Kahn, D.; Phelps, S.; Davies, K.; Gillis, J. M., Expression of truncated utrophin leads to major functional improvements in dystrophin-deficient muscles of mice. *Nat. Med.* **1997,** *3* (11), 1216-21.
16. Kleopa, K. A.; Drousiotou, A.; Mavrikiou, E.; Ormiston, A.; Kyriakides, T., Naturally occurring utrophin correlates with disease severity in Duchenne muscular dystrophy. *Hum. Mol. Genet.* **2006,** *15* (10), 1623-8.
17. Chancellor, D. R.; Davies, K. E.; De Moor, O.; Dorgan, C. R.; Johnson, P. D.; Lambert, A. G.; Lawrence, D.; Lecci, C.; Maillol, C.; Middleton, P. J.; Nugent, G.; Poignant, S. D.; Potter, A. C.; Price, P. D.; Pye, R. J.; Storer, R.; Tinsley, J. M.; van Well, R.; Vickers, R.; Vile, J.; Wilkes, F. J.; Wilson, F. X.; Wren, S. P.; Wynne, G. M., Discovery of 2-Arylbenzoxazoles as Upregulators of Utrophin Production for the Treatment of Duchenne Muscular Dystrophy. *J. Med. Chem.* **2011,** *54* (9), 3241-3250.
18. Babbs, A.; Berg, A.; Chatzopoulou, M.; Davies, K. E.; Davies, S. G.; Edwards, B.; Elsey, D. J.; Emer, E.; Guiraud, S.; Harriman, S.; Lecci, C.; Moir, L.; Peters, D.; Robinson, N.; Rowley, J. A.; Russell, A. J.; Squire, S. E.; Tinsley, J. M.; Wilson, F. X.; Wynne, G. M., 2-Arylbenzo[d]oxazole Phosphinate Esters as Second-Generation Modulators of Utrophin for the Treatment of Duchenne Muscular Dystrophy. *J. Med. Chem.* **2020,** *63* (14), 7880-7891.
19. Wilkinson, I. V. L.; Perkins, K. J.; Dugdale, H.; Moir, L.; Vuorinen, A.; Chatzopoulou, M.; Squire, S. E.; Monecke, S.; Lomow, A.; Geese, M.; Charles, P. D.; Burch, P.; Tinsley, J. M.; Wynne, G. M.; Davies, S. G.; Wilson, F. X.; Rastinejad, F.; Mohammed, S.; Davies, K. E.; Russell, A. J., Chemical Proteomics and Phenotypic Profiling Identifies the Aryl Hydrocarbon Receptor as a Molecular Target of the Utrophin Modulator Ezutromid. *Angew. Chem. Int. Ed.* **2020,** *59* (6), 2420-2428.
20. Moorwood, C.; Lozynska, O.; Suri, N.; Napper, A. D.; Diamond, S. L.; Khurana, T. S., Drug discovery for Duchenne muscular dystrophy via utrophin promoter activation screening. *PLOS ONE.* **2011,** *6* (10), e26169.
21. Gordon, B. S.; Delgado Díaz, D. C.; Kostek, M. C., Resveratrol decreases inflammation and increases utrophin gene expression in the mdx mouse model of Duchenne muscular dystrophy. *Clin. Nutr.* **2013,** *32* (1), 104-11.
22. Choi, I. Y.; Lim, H.; Estrellas, K.; Mula, J.; Cohen, T. V.; Zhang, Y.; Donnelly, C. J.; Richard, J. P.; Kim, Y. J.; Kim, H.; Kazuki, Y.; Oshimura, M.; Li, H. L.; Hotta, A.; Rothstein, J.; Maragakis, N.;

Wagner, K. R.; Lee, G., Concordant but Varied Phenotypes among Duchenne Muscular Dystrophy Patient-Specific Myoblasts Derived using a Human iPSC-Based Model. *Cell. Rep.* **2016,** *15* (10), 2301-2312.

23. Bentzinger, C. F.; Wang, Y. X.; Rudnicki, M. A., Building muscle: molecular regulation of myogenesis. *Cold Spring Harb. Perspect. Biol.* **2012,** *4* (2).
24. Kimura, E.; Han, J. J.; Li, S.; Fall, B.; Ra, J.; Haraguchi, M.; Tapscott, S. J.; Chamberlain, J. S., Cell-lineage regulated myogenesis for dystrophin replacement: a novel therapeutic approach for treatment of muscular dystrophy. *Hum. Mol. Genet.* **2008,** *17* (16), 2507-2517.
25. Malik, V.; Rodino-Klapac, L. R.; Mendell, J. R., Emerging drugs for Duchenne muscular dystrophy. *Expert. Opin. Emerg. Drugs.* **2012,** *17* (2), 261-77.
26. Smith, K. J.; Murray, I. A.; Tanos, R.; Tellew, J.; Boitano, A. E.; Bisson, W. H.; Kolluri, S. K.; Cooke, M. P.; Perdew, G. H., Identification of a high-affinity ligand that exhibits complete aryl hydrocarbon receptor antagonism. *J. Pharmacol. Exp. Ther.* **2011,** *338* (1), 318-327.
27. Fang, Z. Z.; Krausz, K. W.; Nagaoka, K.; Tanaka, N.; Gowda, K.; Amin, S. G.; Perdew, G. H.; Gonzalez, F. J., In vivo effects of the pure aryl hydrocarbon receptor antagonist GNF-351 after oral administration are limited to the gastrointestinal tract. *British. J. Pharmacol.* **2014,** *171* (7), 1735-46.
28. Vasbinder, M. M.; Aquila, B.; Augustin, M.; Chen, H.; Cheung, T.; Cook, D.; Drew, L.; Fauber, B. P.; Glossop, S.; Grondine, M.; Hennessy, E.; Johannes, J.; Lee, S.; Lyne, P.; Mörtl, M.; Omer, C.; Palakurthi, S.; Pontz, T.; Read, J.; Sha, L.; Shen, M.; Steinbacher, S.; Wang, H.; Wu, A.; Ye, M., Discovery and Optimization of a Novel Series of Potent Mutant B-RafV600E Selective Kinase Inhibitors. *J. Med. Chem.* **2013,** *56* (5), 1996-2015.
29. Smith, A. L.; Andrews, K. L.; Beckmann, H.; Bellon, S. F.; Beltran, P. J.; Booker, S.; Chen, H.; Chung, Y.-A.; D'Angelo, N. D.; Dao, J.; Dellamaggiore, K. R.; Jaeckel, P.; Kendall, R.; Labitzke, K.; Long, A. M.; Materna-Reichelt, S.; Mitchell, P.; Norman, M. H.; Powers, D.; Rose, M.; Shaffer, P. L.; Wu, M. M.; Lipford, J. R., Discovery of 1H-Pyrazol-3(2H)-ones as Potent and Selective Inhibitors of Protein Kinase R-like Endoplasmic Reticulum Kinase (PERK). *J. Med. Chem.* **2015,** *58* (3), 1426-1441.
30. Van Horn, K. S.; Zhu, X.; Pandharkar, T.; Yang, S.; Vesely, B.; Vanaerschot, M.; Dujardin, J.-C.; Rijal, S.; Kyle, D. E.; Wang, M. Z.; Werbovetz, K. A.; Manetsch, R., Antileishmanial Activity of a Series of N2,N4-Disubstituted Quinazoline-2,4-diamines. *J. Med. Chem.* **2014,** *57* (12), 5141-5156.
31. Huang, C.; Tang, X.; Fu, H.; Jiang, Y.; Zhao, Y., Proline/Pipecolinic Acid-Promoted Copper-Catalyzed P-Arylation. *J. Org. Chem.* **2006,** *71* (13), 5020-5022.
32. Inglis, S. R.; Stojkoski, C.; Branson, K. M.; Cawthray, J. F.; Fritz, D.; Wiadrowski, E.; Pyke, S. M.; Booker, G. W., Identification and Specificity Studies of Small-Molecule Ligands for SH3 Protein Domains. *J. Med. Chem.* **2004,** *47* (22), 5405-5417.
33. Martin, S. C.; Ball, Z. T., Aminoquinoline–Rhodium(II) Conjugates as Src-Family SH3 Ligands. *ACS Med. Chem. Lett.* **2019,** *10* (10), 1380-1385.
34. Henry, E. C.; Bemis, J. C.; Henry, O.; Kende, A. S.; Gasiewicz, T. A., A potential endogenous ligand for the aryl hydrocarbon receptor has potent agonist activity in vitro and in vivo. *Arch. Biochem. Biophys.* **2006,** *450* (1), 67-77.
35. Xie, H. Q.; Xia, Y.; Xu, T.; Chen, Y.; Fu, H.; Li, Y.; Luo, Y.; Xu, L.; Tsim, K. W. K.; Zhao, B., 2,3,7,8-Tetrachlorodibenzo-p-dioxin induces alterations in myogenic differentiation of C2C12 cells. *Environ. Pollut.* **2018,** *235*, 965-973.
36. Di, L.; Kerns, E. H., Profiling drug-like properties in discovery research. *Curr. Opin. Chem. Biol.* **2003,** *7* (3), 402-408.
37. Mallesh, R.; Khan, J.; Pradhan, K.; Roy, R.; Jana, N. R.; Jaisankar, P.; Ghosh, S., Design and Development of Benzothiazole-Based Fluorescent Probes for Selective Detection of Aβ Aggregates in Alzheimer's Disease. *ACS Chem. Neurosci.* **2022,** *13* (16), 2503-2516.
38. Péladeau, C.; Adam, N.; Bronicki, L. M.; Coriati, A.; Thabet, M.; Al-Rewashdy, H.; Vanstone, J.; Mears, A.; Renaud, J. M.; Holcik, M.; Jasmin, B. J., Identification of therapeutics that target eEF1A2 and upregulate utrophin A translation in dystrophic muscles. *Nat. Commun.* **2020,** *11* (1), 1990.

39. Gupta, V.; Mahata, T.; Roy, R.; Gharai, P. K.; Jana, A.; Garg, S.; Ghosh, S., Discovery of imidazole-based GSK-3β inhibitors for transdifferentiation of human mesenchymal stem cells to neurons: A potential single-molecule neurotherapeutic foresight. *Front. Mol. Neurosci.* **2022,** *15*, 1002419.
40. Livak, K. J.; Schmittgen, T. D., Analysis of relative gene expression data using real-time quantitative PCR and the 2(-Delta Delta C(T)) Method. *Methods.* **2001,** *25* (4), 402-8.
41. Denes, L. T.; Riley, L. A.; Mijares, J. R.; Arboleda, J. D.; McKee, K.; Esser, K. A.; Wang, E. T. Culturing C2C12 myotubes on micromolded gelatin hydrogels accelerates myotube maturation. *Skelet. Muscle.* , **2019**, *9* (1), 1-10.

42. Di, L.; Kerns, E. H.; Hong, Y.; Kleintop, T. A.; McConnell, O. J.; Huryn, D. M., Optimization of a higher throughput microsomal stability screening assay for profiling drug discovery candidates. *J. Biomol. Screen.* **2003,** *8* (4), 453-62.

43. Kerns, E. H.; Di, L., Automation in Pharmaceutical Profiling. *JALA: J. Lab. Autom.* **2005,** *10* (2), 114-123.

44. Konsoula, R.; Jung, M., In vitro plasma stability, permeability and solubility of mercaptoacetamide histone deacetylase inhibitors. *Int. J. Pharm.* **2008,** *361* (1-2), 19-25.

45. Wenlock, M. C.; Potter, T.; Barton, P.; Austin, R. P., A method for measuring the lipophilicity of compounds in mixtures of 10. *J. Biomol. Screen.* **2011,** *16* (3), 348-55.